Master Thesis

Evaluation of an SMC powder during uniaxial compaction and subsequent annealing treatment

carried out for the purpose of obtaining the degree of Master of Science (MSc or Dipl.-Ing or DI), submitted at TU Wien, Faculty of Technical Chemistry, by

Anna Lebhard

Mat.Nr.: 01305063

under the supervision of

Ass. Prof. Dipl.-Ing. Dr. techn. Christian Gierl-Mayer

Institute of Chemical Technologies and Analytics, E164-03-3

Vienna, January 2021

This work was supported by Huawei Technologies Düsseldorf GmbH within the framework of the project “Evaluation of an SMC powder during uniaxial compaction and subsequent annealing treatment” under the agreement No. YBN2019075010.

Affidavit

I declare in lieu of oath, that I wrote this thesis and performed the associated research myself, using only literature cited in this volume. If text passages from sources are used literally, they are marked as such.

I confirm that this work is original and has not been submitted elsewhere for any examination, nor is it currently under consideration for a thesis elsewhere.

I acknowledge that the submitted work will be checked electronically-technically using suitable and state-of-the-art means (plagiarism detection software). On the one hand, this ensures that the submitted work was prepared according to the high-quality standards within the applicable rules to ensure good scientific practice "Code of Conduct" at the TU Wien. On the other hand, a comparison with other student theses avoids violations of my personal copyright.

Abstract

SMCs (Soft Magnetic Composites) offer new promising prospects for mid-range frequency electromagnetic applications. Produced by efficient powdermetallurgical methods, they not only show remarkable magnetic and electric properties, but have also proven to be able to compete with well-established materials like laminated steel sheets.

The goal of this thesis was the production of stable samples from a SMC powder, supplied by Huawei, by uniaxial compaction and subsequent annealing treatment. Furthermore, the optimisation of the electromagnetic performance of the samples was aimed for by adjusting the production and annealing parameters.

Various compaction trials were conducted to find a suitable pressing aid and determine the ideal compaction pressure. To increase the mechanical strength of the samples even further, a post-processing step, which includes the impregnation of the samples with an adhesive, was introduced.

Further trials were conducted to evaluate the effect of the duration and temperature level of an annealing treatment on the most important parameters (magnetic saturation, coercitivity, specific resistivity and transverse rupture strength).

Furthermore, the properties of the powder itself were evaluated by elemental analysis, differential thermoanalysis, measurement of particle size distribution and X-Ray Photoelectron Spectroscopy and consequently a theory for a mechanism was proposed, which explains the increase in specific resistivity at elevated annealing temperatures.

It was shown that, at the right conditions, production of stable and well-performing samples from the given Fe-Si powder is feasible. Moreover, these samples offer properties which can compete with other commercially available SMC powders.

Kurzfassung

SMC (=Soft magnetic composite)-Werkstoffe bieten für elektromagnetische Anwendungen eine innovative, pulvermetallurgische Alternative zu den bereits etablierten, laminierten Blechen, da sie, vor allem im hochfrequenten Anwendungsbereich, eine hohe Leistung bei geringen Energieverlusten aufweisen.

Ziel dieser Arbeit war es durch uniaxiales Pressen und anschließender Wärmebehandlung ein stabiles Bauteil aus einem SMC-Pulver (in diesem Fall ein Fe-Si-Pulver mit elektrisch isolierender Schicht) herzustellen und dabei die magnetischen und elektrischen Eigenschaften zu optimieren.

Durch verschiedene Pressversuche wurde empirisch ein geeignetes Presshilfsmittel und der ideale Pressdruck ermittelt. Zur Erhöhung der Stabilität wurden die Bauteile nach der Temperaturbehandlung mit einem geeigneten Klebstoff imprägniert.

Weiters wurden durch Herstellung und Untersuchung mehrerer Probenserien, die in der Höhe und Dauer der Temperaturbehandlung variieren, der Einfluss dieser auf leistungsbestimmende Parameter (Magnetische Sättigung, Koerzitivfeldstärke, spezifischer Widerstand und Biegefestigkeit) untersucht und diese auch maßgeblich verbessert. Außerdem wurden durch Elementaranalyse, Differentielle Thermoanalyse, Messung der Partikelgrößen und XPS (X-Ray Photoelectronspectroscopy)-Messungen nicht nur Informationen über das bereitgestellte Pulver gesammelt, sondern auch ein Mechanismus vorgeschlagen, der bei den hergestellten Werkstücken zur Erhöhung des elektrischen Widerstandes bei erhöhten Temperaturen führt.

Folglich wurde gezeigt, dass bei den passenden Bedingungen Werkstücke aus dem Fe-Si-Pulver hergestellt werden können, die in Bezug auf mechanische und elektromagnetische Leistung vergleichbar gut wie andere kommerziell erhältliche SMC-Pulver abschneiden.

Acknowledgments

I am very grateful for all the support I received during my master thesis.

First of all, I want to thank my supervisor Ass. Prof. Dr. Christian Gierl-Mayer, who not only gave me the opportunity to work on this thesis, but also offered his valuable advice and guidance when needed and tackled encountered problems with a positive and encouraging attitude. Furthermore, I want to thank Univ. Prof. Dr. Herbert Danninger, who contributed to this work with his expertise and counsel.

Also, I want to thank my colleagues, who helped me countless times during my work and who created a friendly and supportive atmosphere, which made every day more enjoyable.

Lastly, I want to express my gratitude to my family, especially my parents, my boyfriend and my friends for the unconditional support during the last years.

Contents

1 Introduction

The growing importance of electromagnetic machinery in the modern world demands for the development and optimisation of suitable materials and efficient technologies. Especially in times of climate change, the focus on efficiency is even reinforced and challenges scientific research to not only look at new inventions, but also to reassess prevailing and well-established technologies. An important factor of the development of electromagnetic parts is the availability of suitable magnetic materials [1].

During the last several years, new materials with interesting properties and features emerged. One of these are the so-called *Soft Magnetic Composites,* or *SMCs*. Their magnetic properties make them a promising candidate for the construction of electromagnetic components, especially if used in mid-frequency applications [2].

This thesis will discuss a potential SMC candidate, a Fe-Si powder supplied by Huawei. The goal was to find an efficient route to produce samples for electromagnetic purposes from the powder by uniaxial compaction and subsequent annealing treatment and to evaluate the effect of the processing parameters on mechanical and magnetic properties.

Another aim was to characterise the powder itself to consider the effect of the powder properties on the overall performance of the samples.

2 Theoretical Background

2.1 Powder metallurgy

Powder metallurgy is a branch of metallurgy which aims to produce materials from metal powders. One conventional route of sample production is the uniaxial compaction of the powder. Essential for this type of processing are the five following steps: Powder manufacture, mixing/blending, uniaxial compaction, sintering and final treatment. Also other branches of PM have gained a lot of importance, e.g. Hot-isostatic pressing (HIP), Metal Injected Molding (MIM) or Additive Manufacturing (AM).

2.1.1 Application and advantages of powder metallurgy

The commercial use of powder metallurgy began about 1900 with the industrial production of tungsten and molybdenum. At the time powder metallurgy was the only way to process these metals, as electric arc furnaces had not been developed yet. As a result, powder metallurgy gained importance when conventional metallurgical routes seemed to fail. Even though technological progress has been made over the last century, its importance remains, as there are still various materials and parts which cannot be produced efficiently with common melting routes.
Nowadays PM is used, for example for the production of porous materials, which are highly demanded as filters, self-lubricating bearings or electrodes. It also enables the production of composite materials of metals, which are not mutually miscible in the liquid condition due to a large difference of the melting points (e.g. W-Cu, W-Ag and Ag-CdO for electric contacts).

Powder metallurgical techniques can be applied to nearly every metal and alloy and therefore offer a wide range of application fields with only little constraints.
Targeted towards mass production, they also enable economic and cost-effective production. The near-net shape compaction of powders while maintaining adequate surface finishing minimises or even eliminates additional machining steps like shape cutting. Compared to conventional metal shaping methods like forging and casting this does not only reduce scrap losses, but also makes manufacturing of complex geometries at a high production rate and low costs possible. The properties of the produced parts can be tailored to the needs and demands of the user [3, 4].

2.1.2 Powder production

The first crucial step to a PM part is the powder production. The production parameters of a powder determine the final shape and composition, which directly influence the properties and quality of the final metal parts. Mechanical and (electro-) chemical methods can be applied for powder production.

2.1.2.1 Mechanical communition without phase transformation

A solid material is milled into particles. The kinetic energy, which originates from the motion of a mill, is transferred onto the particles either by the material itself or by foreign bodies (e.g. balls in a ball mill). The impact on the material causes strain which eventually leads to disintegration of the supplied material [3].
For mechanochemical production of metal powders a variety of different methods and equipment setups are known and used, the most common one being ball mills, vibration mills

or attritors. Therefore, milling comprises a versatile method of powder production. The process is simple and easy to upscale for industrial manufacturing. However, mechanical comminution requires a lot of energy, which increases processing time and costs. Another major concern is the contamination of the powder caused by the wear and tear of the milling tools [5].

2.1.2.2 Atomisation/Mechanical disintegration with phase transformation

With this method, a melt of a metal or alloy is dispersed, e.g. by pressure gas, pressure liquid, ultrasound, or centrifugal force. The goal is to break up the melt into small droplets which are rapidly cooled down to form a powder. The properties of the powder can be varied by the type of dispersion, the energy acting on the melt, the temperature and viscosity of the melt and the cooling conditions [6].

2.1.2.2.1 Water atomisation

In this technique a melt is lead through a nozzle and dispersed by water jets. It is a common method to produce iron and steel powders, which yields irregularly shaped particles for high compressibility, and a low carbon content. The particle size can be adjusted by different water pressures. The produced powders have to undergo subsequent annealing treatment in reducing H_2-atmosphere as the metal reacts with the oxygen during the jetting process [6].

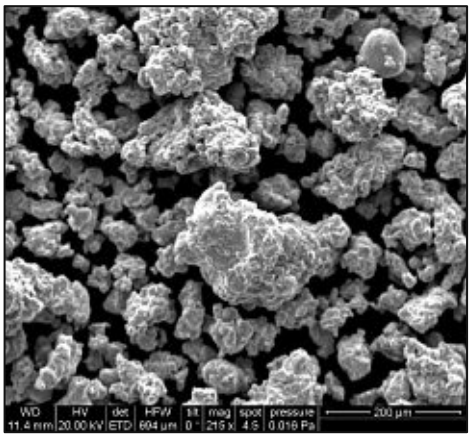

Figure 1 Water-atomised iron powder (ASC 100.29, Höganäs AB)

2.1.2.2.2 Gas atomisation

Similar to water atomisation, a melt is hit by gas jets after emerging from a nozzle.

Usually inert gases are used for this purpose, e.g. N_2 and argon. This type of atomisation is very costly, but it manages to yield round shaped powders which reach high bulk densities and are therefore ideal for HIP and AM. It is also the method of choice for clean powder production of reactive alloys, as the inert atmosphere prevents oxidation. Problems can arise due to the formation of so-called satellites, which are undesirable for many uses (see Figure 2) [6].

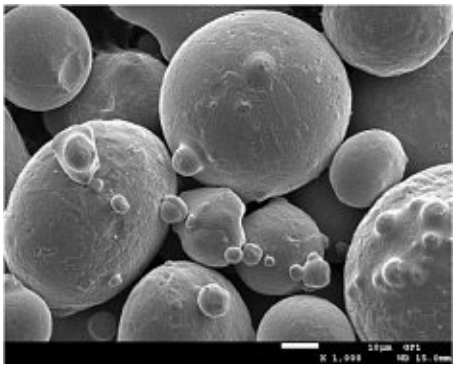

Figure 2 Gas-atomised steel powder (UNS 17400) with typical satellite structure [7]

2.2 Magnetism

Before introducing Soft Magnetic Composites and their key features, a short introduction on magnetism and magnetic properties will be given.

A magnetic field can be described by its induction B [T] or the field strength H [A/m]. In a vacuum they relate as follows (with the vacuum permeability $\mu_0 = 4\pi \cdot 10^{-7}$ Vs/Am):

$$B = \mu_0 H \quad (1)$$

If a specimen is inserted into a magnetic field, the induction and field strength of the externally applied magnetic field B_{ext} will either decrease or increase inside of the specimen to B_{int}. The extent of this behaviour is described by the permeability μ and the susceptibility χ of a material. The lack or excess of magnetic induction in a material compared to an outer field can be described as the magnetic polarisation J [T].

$$B_{int} = \mu B_{ext} \quad (2)$$

$$B_{int} = B_{ext} + J \quad (3)$$

$$J = \chi B_{ext} \quad (4)$$

Additionally, the magnetisation *M* [A/m] of a material can be described as:

$$M = \chi H_{ext} \quad (5)$$

$$J = \mu_0 M \quad (6)$$

According to their magnetic behaviour, measured in the above-mentioned values, materials can be divided into diamagnetic, paramagnetic and ferromagnetic.

2.2.1 Diamagnetism

μ < 1, χ < 0

Every material which consists of atoms, ions or molecules with filled shells and subshells is diamagnetic, as they do not own unpaired electrons and the spin and orbital moments compensate each other. Therefore, no magnetic moment occurs .

A diamagnetic specimen will be repelled by an externally applied field as the induced magnetic polarisation will oppose this field. An external magnetic field will be mitigated in a diamagnetic specimen.

2.2.2 Paramagnetism

μ > 1, χ > 0

If a materials atoms, ions or molecules own unpaired electrons it exhibits a permanent

magnetic moment. Without an external field the moments are statistically distributed and compensate each other, so the material will show no visible effect. When a paramagnetic specimen is brought into an external field, the magnetic moments will align in direction of the field, producing a field oriented in the same direction as the external field. Therefore, the field strength and the induction will increase.

2.2.3 Magnetisation by spin alignment

In diamagnetic and paramagnetic materials no magnetic interaction between the atoms, ions or molecules occurs. In certain groups of materials those spin-spin interactions exist, which leads to a spontaneous magnetisation. The alignment of magnetic spins takes place without applying an external field. Heating above a critical temperature (Curie temperature T_c) leads to a reversible collapse of this spontaneous magnetisation.

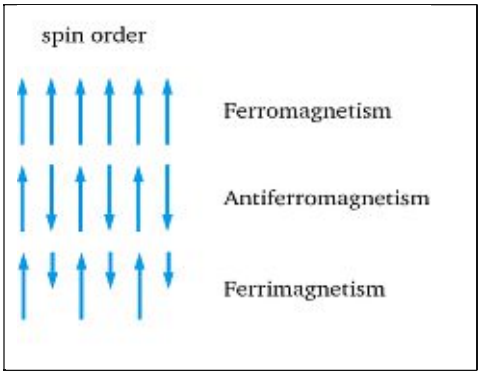

Figure 3 Different types of spin order [8]

According to the nature of the spin alignment different orders can be distinguished. The most important ones are pictured in Figure 3.

2.2.3.1 Ferromagnetism

$\mu >> 1, \chi >> 0$ (typically 10^4 - 10^5)

In ferromagnetic samples the spin moments will align parallel to each other spontaneously within small domains. Above the Curie-Temperature T_C this spin order collapses. Still a ferromagnetic specimen does not exhibit observable magnetic behaviour below T_C, as the direction of magnetisation varies between the magnetic domains and are distributed statistically, hence compensating each other.

In a magnetic field a ferromagnetic material gets magnetised as the magnetic moments from the domains align along that field.

Figure 4 shows the behaviour of a ferromagnetic specimen in an external field. With increasing magnetising force (field strength) the induction B (and therefore the magnetisation M) grows until the aligning of the spins is completed, at which point the Saturation Magnetisation M_S and B_{max} is reached. If, after magnetisation, the field strength again drops to zero a certain amount of magnetisation remains, called the remanence or retentivity. To lower the magnetisation again to zero, a field in the opposite

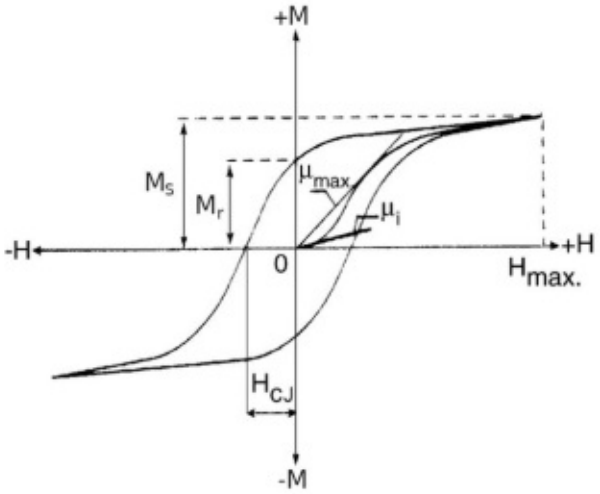

Figure 4 Hysteresis curve of a ferromagnetic specimen [9]

direction must be applied. The force of the field that is needed to eliminate the remanence is referred to as the coercivity H_{CJ} [8]. Materials that own a high coercivity are called *hard magnets* while those with a low coercivity are called *soft magnets*. Figure 5 shows a comparison between the theoretical hysteresis loops of a soft and a hard magnetic material.

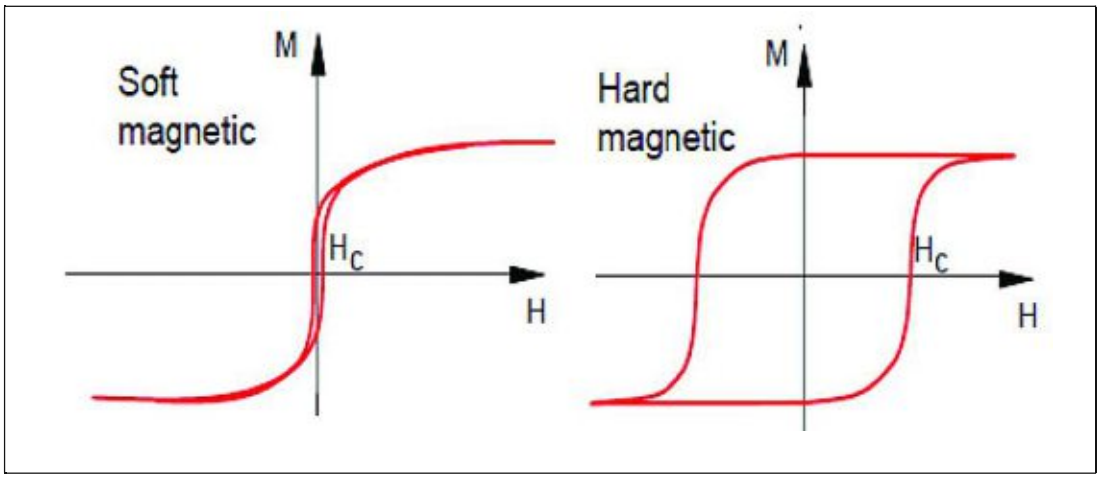

Figure 5 Comparison of hysteresis curves of a soft and a hard magnet [10]

A hard magnet can only be demagnetised by a high field strength; therefore, they are used as permanent magnets, e.g. for motor applications or as actuators. The terms *hard* and *soft* magnets originated from the mechanical properties of the corresponding magnetic steels, as hardened (=martensitic) steels are known to show typical hard magnetic behaviour. Further examples for permanent magnets are ferrites, NdFeB or SmCo.

Compared to hard magnets, soft magnets show a significantly lower remanence and coercivity and therefore demagnetise rather easily.
They are widely used for power generation, condition, transfer, and conversion, as well as in electric machines, power electronics, sensors, and electromagnetic interference (EMI) preventions.

Examples for soft magnetic materials are iron, soft ferrites, electrical steels (Fe-Si alloys) or Fe-Ni alloys [11].

Prior to a more detailed description of the most common soft magnetic materials, the mechanism of magnetic losses, which is dependent on the material used, needs to be discussed.

2.2.3.1.1 Magnetic losses

Magnetic losses play an important role during the magnetisation and demagnetisation cycle of soft magnets. These are caused by various mechanisms, which lead to the dissipation of energy via heat. The extent of these losses is one of the main criteria for a well-suited choice of magnetic material. Three main types of magnetic losses can be distinguished:

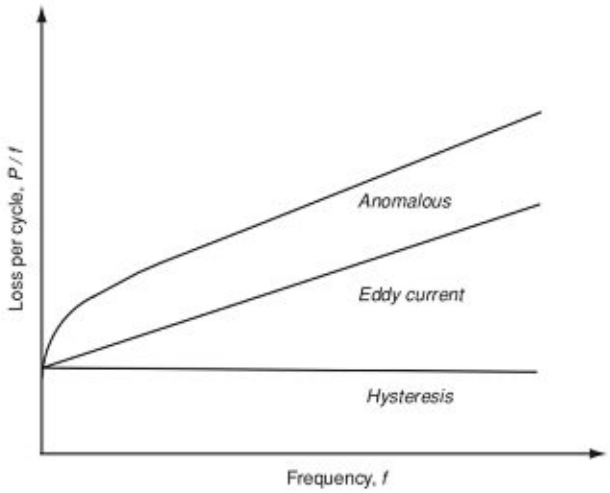

Figure 6 Correlation of magnetic losses and frequency [11]

- Hysteresis loss P_{hy}
- Eddy-current loss P_{ed}
- Anomalous loss P_{an}

The total loss P_{tot} of a material is the sum of the three mentioned losses.

$$P_{tot} = P_{hy} + P_{ed} + P_{an} \qquad 7$$

Hysteresis loss is caused by the movement of the domain walls during the magnetisation/demagnetisation loop. Anything acting as a barrier towards this movement, e.g. impurities, dislocations or grain boundaries, increases the hysteresis losses [12]. The hysteresis loss of a material is given by the area of the B(H) loop or μ_0M(H') loop, described by the following formula, at a frequency f [11]:

$$P_{hy} = f\ \mu_0 \int_{loop} H' dM \qquad 8$$

Eddy-current losses occur due to the fluctuating magnetic field, which generates stray electric currents. Eddy-currents pose an important challenge especially in high-frequency applications, as P_{ed} increases with the square of the frequency [12].

$$P_{ed} = \frac{(\pi\ t\ f\ B_{max})^2}{6\ \varrho} \qquad 9$$

Anomalous losses are also called residual losses, as they are mostly measured by the difference of theoretical and experimental results. They are caused by extra-eddy current losses due to domain wall motion, non-uniform magnetisation, and sample inhomogeneity. This type of losses also increases with rising frequency [12].

$$P_{an} = \frac{(4\,f\,B_{max})^2 dt}{\pi \varrho} \sum_{n\ odd} \frac{1}{n^3} \coth\left(\frac{n\,\pi\,d}{t}\right) \qquad 10$$

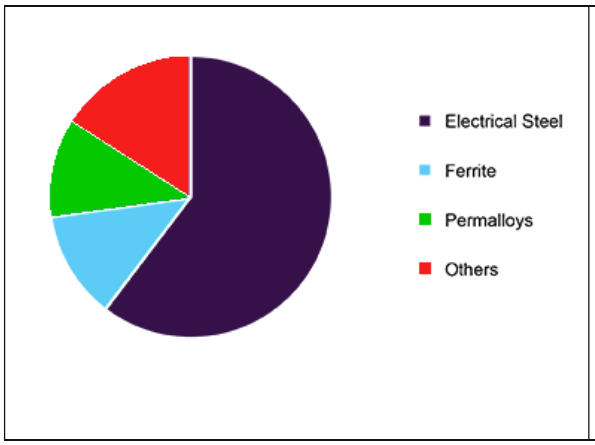

Figure 7 Global soft magnetic material market share in 2019 (redrawn from [13])

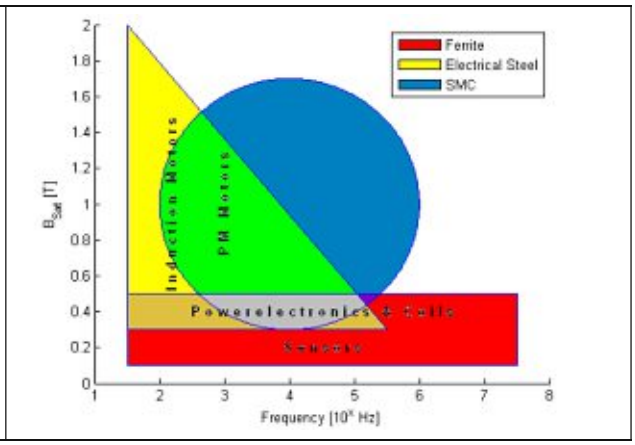

Figure 8 Application areas of ferrites, electrical steel and SMC for different frequencies and saturation flux densities [14]

For different purposes one must choose between various soft magnetic materials and consider their trade-off between losses, polarisation, permeability, and cost. While core losses should be kept at a minimum, the polarisation should be as large as possible for a given excitation field.

Examples of well-known soft magnetic materials largely used for commercial applications are soft ferrites, electric steels (Fe-Si alloys) or permalloys (nickel-iron alloy). Figure 8 shows the performance areas for ferrites, electrical steel, and soft magnetic composites (SMC). While electrical steels and ferrites have been known and used for a long time and still remain beneath the most important classes of soft magnetic materials (see Figure 7), the more novel SMCs begin to grow in importance as they may cover applications areas, where other materials still cannot offer a perfect trade-off.

2.3 Ferrites

Soft ferrites have a cubic crystal structure and the general formula $MO{\cdot}Fe_2O_3$, where M is a divalent metal such as Mg, Mn, or Ni. Nonmagnetic Zn ferrite is often added to increase the saturation magnetisation M_S. Most of the commercial ferrites are mixed ferrites (solid solutions of one ferrite in another).

Ferrites only reach low M_S values (about a third of iron and its alloys), low permeabilities and low densities (just above 5 g/cm^3), which makes them unsuited for applications in static or moderate-frequency field. Their importance as soft magnetic material manifested with their extremely high electrical resistivity, which provides minimum eddy-current losses. Therefore they are the most important material for high frequency applications [15].

2.4 Electrical steel

The magnetic properties of iron in general can be optimised for electromagnetic applications by adding Si, C, P, Al and some other elements . An example for a widely used soft magnetic steel is electrical steel, which is an iron alloy with a silicon content up to 6.5%. Silicon is a suitable candidate for alloying, as it reduces the coercivity and increases the resistivity almost linearly to its concentration. For instance, a silicon addition of 3wt% raises the resistivity of plain iron from 8.6 µΩcm to about 50 µΩcm.[9, 16] This subsequently leads to lower core losses. However, silicon addition also increases its hardness and brittleness, therefore it cannot be increased randomly [3].

Alloys with addition of 1-4% silicon and manufactured as sheets are the predominantly used material for transformers and electromagnetic machinery.

Electrical steel sheets are distinguished between grain-oriented and non-oriented electrical steels. Grain-oriented steel has anisotropic magnetic property to the rolling direction and is mainly used in static machinery, which requires unidirectional magnetisation, e.g. transformers. Non-oriented steel has isotropic magnetic property in all directions and is therefore mainly used in rotating machinery which requires multidirectional magnetisation, e.g. motors and generators [17].

Electrical steel sheets are often used as a stack of laminated sheets. By constructing a specimen, which is assembled from several electrically insulated sheets, eddy-currents can be reduced significantly. This is especially important with increasing frequencies, as the eddy current losses increase with squared frequency. This method has been widely used for the production of transformer cores [11].

2.5 Soft magnetic composites

A relatively new approach is the manufacturing of composite materials through powder metallurgical processes by compaction of powders with an electrically insulating coating. The concept is similar to the lamination of steel sheets: By coating an iron powder with an electrically insulating coating the eddy-currents in a compacted sample dissipate, and the losses decrease [2].

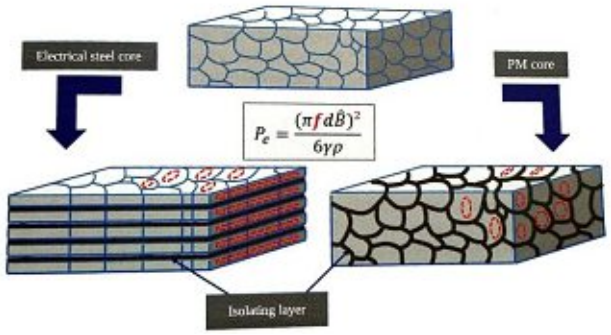

Figure 9 Reduction of eddy-currents by lamination or powder coating [18]

2.5.1 Processing of SMC

The manufacturing process is almost the same as for regular powder metallurgical parts. The base material usually consists of plain iron or low-alloyed (Si, Ni, Al…) iron-based powder. The powders are preferably produced by water-atomisation to ensure adequate compressibility.

Those are then coated and, if necessary mixed with a lubricant or other required additives. Eventually the powder is compacted to a near-net shape, and in a final step annealed.

In SMC technology, annealing treatments are usually conducted at lower temperatures (typically 200-700°C) than in the usual sintering process to prevent the direct disintegration of the coating and the formation of necks between adjacent particles, which is aimed for in sintering [12]. These necks would eliminate the insulating effect of the powder coating and increase the conductivity of the parts . This effect is demonstrated by the decrease of electrical resistivity of plain iron powder with rising sintering temperatures [19]. The purpose of the annealing treatment is relieving the stress on the particles, induced by compaction at high pressures, but due to the upper temperature limit the stress–relief often cannot be completed for some powder/coating-combinations, as the typical stress–relief temperature for plain iron is between 570–775°C [12].

2.5.1.1 Powder coatings

The processing of the SMC powders is largely determined by the nature of the coating, which can be roughly divided into organic and inorganic.

- Polymers pose a convenient option for organic coatings for SMC powders. Besides the insulating effect, they also act as a binder medium, which provides stability and improves the mechanical properties of manufactured parts. However, the applied amount of polymer has to be kept at a minimum, as higher amounts reduce the permeability.
  Polymers coatings, for instance epoxy and phenolic based resins, are mostly applied by dissolving in a solvent, mixing with the powder, and drying until complete evaporation of the solvent [20-22]. In some cases, dry blending of the powder with the polymer also works sufficiently [23, 24].
- Typical inorganic coatings for SMC include phosphates (zinc/iron/manganese phosphates), oxides, and sulfates. Those are usually applied to the powders by either wet chemical or dry chemical methods. Wet chemical application works by precipitating a suitable inorganic layer (e.g. Fe–Zn phosphate) on the metallic surface. In the dry chemical method, the metallic powders are, for example, oxidised in a furnace at a suitable temperature and atmosphere to create an insulating oxide layer [25].

2.5.2 Advantages of SMC

The powder metallurgical manufacturing of SMC parts offers several advantages. The near-net shape production with little to no postprocessing leads to time- and cost-effective production. Besides these economic advantages, it also leads directly to less environmental impact. Nowadays the development of sustainable and “green” methods is highly requested. Powder metallurgy in general is recognised as a green technology, because the manufacturing steps save energy and reduce scrap waste [26].
The near-net shape technique also enables the production of parts with complex geometries. These can be designed with only little limitations to fulfil various requirements. Another major advantage is the anisotropic structure of the powder cores, which allows for more application possibilities. For example, compared to currently used electrical steel cores in motor applications laminated steels are restricted to 2D-magnetic flux applications perpendicular to the laminations to decrease eddy-currents, while the powder core can also be used for transversal flux motors, which need 3D magnetic directions.

More benefits arise from the comparably little physical impact of the PM route. The manufacturing process always has a strong effect on the properties of a material, especially on the magnetic characteristics. In case of the electrical steels their extensive processing (hot or cold rolling) can cause a deterioration of its magnetic properties. As powder specimens receive their final shape very soon in the manufacturing procedure, the negative impact is kept at a minimum. Moreover, the stress induced by compaction can be cured during an annealing treatment [2].

Besides the mentioned advantages regarding production and application, SMC parts show a better recyclability compared to laminated steels: after usage SMC transformer cores can be shattered easily and separated from the copper windings, while the laminated steel packages have to be shredded, which impairs the isolation of valuable copper [27].

2.5.3 Limitations and future objectives of SMC technology

SMCs are a relatively new technology therefore several issues remain to be improved in the future.
Even though PM techniques show a lot of advantages, they also create various problems. One is the resulting porosity which leads to low density values of the samples. A low density might be desirable for weight-saving purposes, but it negatively impacts magnetic properties such as the permeability and the saturation magnetisation [2, 22].

The density strongly depends on the shape and type of powder used. As already mentioned in chapter 2.1.2, irregularly shaped particles, usually produced by water atomisation, have a higher compressibility and should be preferred for compaction.

Another way of increasing the density of compacted parts might be the application of higher compaction pressures, but higher pressures also induce higher strain on the particles due to the cold working effect on iron and probably damage to the insulating coating [25]. Damages and strain lead to deterioration of magnetic properties and electric insulation. The strain can be partially relieved with a temperature treatment, but, depending on the nature of the insulating coating, the temperatures have to be kept relatively low so complete relieving of the strain might not be possible. Improvements can be achieved by elongating the duration of the heat treatment [12]. Also, magnetic annealing treatment , which consists of applying a magnetic field onto the samples during heat treatment or at room temperature to relieve residual stress, could be a possibility to enhance the magnetic properties [21].

Finally, the materials choice for powder manufacturing has to be considered. While iron-based alloys in general offer acceptable properties, adding other elements (like silicon, phosphorus, nickel,…) could lead to an improvement of electromagnetic performance. However, the overall performance after alloying, including mechanical properties, ageing, and pricing has to be taken into account. Especially the choice for an insulating coating has to be made with caution, as this will greatly influence the determination of the processing parameters [25].

After all, adjustments and trade-offs have to be made in the proceeding of finding the ideal powder.

A lot of effort has already been expended by various research teams around the world to find and improve suitable materials and powders for SMC. However, we are still navigating through a rather novel area of powder metallurgy with new needs and requirements. Therefore, this topic provides a great amount of opportunities for promising future research and development.

3 Sample Preparation

3.1 Fe-Si Powder

For microscopic characterisation the Fe-Si powder was embedded into Struers EpoFix epoxy resin, polished (as described in chapter 3.4) and investigated by optical microscopy, SEM (Scanning electron microscopy) and XRF (X-Ray Fluorescence Spectroscopy).

SEM pictures were taken by distributing the loose powder on a conducting carbon adhesive tape.

A small amount of powder was heated to 600°C for 30min in inert atmosphere (N_2 gas flow at 2l/min) to observe the effect of a heat treatment on the powder and its coating.

Furthermore, the particle size distribution of the as-delivered powder was measured (see 5.1.3).

3.2 Pressing Trials

The first step in this project was to find the ideal way to produce a sample from the given powder by conducting several pressing trials and evaluating the properties of the received samples.

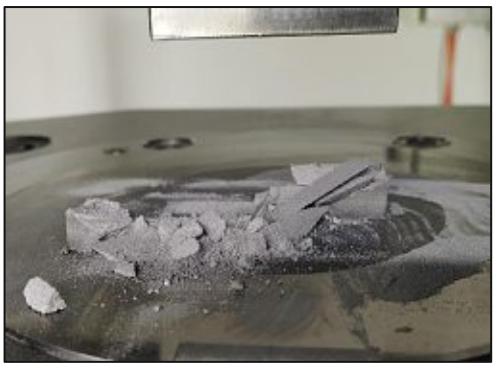

Figure 10: Fe-Si Powder after compaction with 0.6% EBS at 600 MPa

3.2.1 Pre-Trials

As a first approach to compact the powder a standard procedure of pressing metal powders was applied. For this purpose, the coated, gas atomised FeSi powder was mixed with 0.6 wt.% commercial pressing lubricant (EBS, Ethylene-bis-stereoylamide) for 20 minutes, using a WAB Turbula T2F mixer, and compacted at pressures of 200, 400, 600 and 800 MPa. However, it showed that the obtained samples were not stable enough to be handled, they even disintegrated during ejection (see Figure 10) and therefore no results were obtained.

3.2.2 Compaction with 1.8 wt.% EBS

A second series of samples with a higher EBS content of 1.8 wt.% was mixed in the Turbula T2F mixer and compacted at 200, 400, 600 and 800 MPa, respectively. The dimensions and weight of the obtained green samples were measured and afterwards heat treated at 600°C for 30 min in inert atmosphere (N_2 at 2l/min, purity 99.999%; AHT furnace with steel muffle).

The heat-treated samples were investigated through optical microscopy and etching, additionally, density and hardness (HV 0.1) were measured. The samples still showed very low strength and density and had a high tendency for cracking and breakage. This made the handling very problematic, and therefore further measurements could not be conducted (see Figure 11).

Figure 11: Samples pressed with 1.8% EBS at 800, 600, 400 and 200 MPa after heat treatment

3.2.3 Compaction with paraffin

Coated, gas atomised Fe-Si powder was compacted with addition of 0.5 wt%, 0.75 wt% and 1.0 wt% paraffin, respectively. The required amount of paraffin was dissolved in cyclohexane and after addition of the Fe-Si powder to the solution the slurry was wet mixed for 30 minutes using a WAB Turbula T2F mixer. The cyclohexane was then removed in a rotary evaporator until the powder was dry. To avoid agglomeration the dry powder was sieved using a 200 µm sieve. Compacting the powders at 200, 400 and 600 MPa yielded stable samples. The heat treatment, done in inert atmosphere (N_2 at 2 l/min flow rate) consisted of slowly heating the samples up to 600°C with a rate of 1 K per minute and holding this temperature for 1 hour. The low heating rate was necessary to prevent sudden expansion of the pieces from the high amount of evaporating paraffin. Handling was still very critical, and the samples were fragile and easily damaged (see Figure 12).

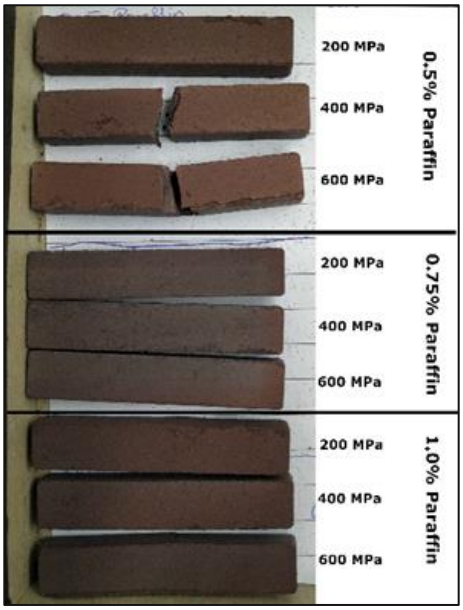

Figure 12: Samples of the first pressing trial with paraffin

For characterisation, optical microscopy, density, hardness (HV 0.1), magnetic saturation and coercivity measurements were conducted. The samples compacted with 0.75% paraffin at 400 MPa appeared to be most stable ones after heat treatment, therefore these were additionally impregnated to increase their stability further (described in chapter 3.5).

3.2.4 Mixing with Somaloy 130i 5P

To gain higher densities and better magnetic properties, the Fe-Si powder was mixed with a different SMC powder (Somaloy 130i 5P, a water-atomised coated iron powder). For this purpose, the Fe-Si powder was mixed with 10%, 20% or 30% Somaloy 130i 5P and 1.0% EBS in the Turbula T2F mixer and compacted at 200, 400 and 600 MPa. The received samples were heated up to 600°C at a rate of 1 K/min and held at this temperature for 1 hour in inert atmosphere (N_2 at 2 l/min).

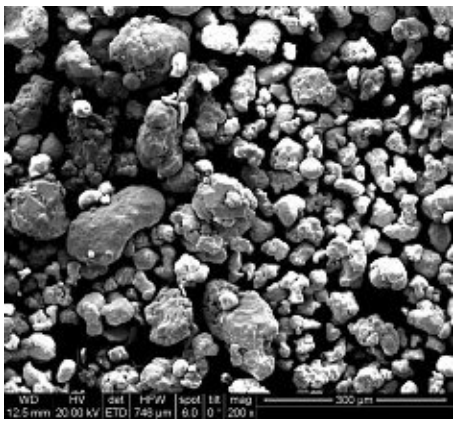

Figure 13 SEM picture of Somaloy 130i 5P, Höganäs [28]

3.3 Annealing Trials

After evaluating the results from the prior pressing trials (see 5.2.1), it was concluded that the best way to produce samples from the given Fe-Si-powder was compaction at 400 MPa with addition of 0.75% paraffin (prepared as described in chapter 3.2.3).
The second step in this project was to optimise the annealing temperature and duration to gain better magnetic and electric performance of the produced parts.
The samples of the annealing trials were evaluated by measuring their density, magnetic saturation coercivity, electric resistivity and transverse rupture strength.

3.3.1 Evaluation of Annealing Temperature

The green parts were produced as described above and annealed at six different temperatures (400, 500, 600, 700, 750 and 800°C in N_2-gas flow at 2l/min). For this purpose, the samples were heated up to a certain temperature at a rate of 2K/min and held at this temperature for one hour. After annealing, the samples were impregnated (see chapter 3.5).

3.3.2 Evaluation of Annealing Duration

The effect of the duration of the annealing treatment was evaluated by heating up the samples to a certain temperature at a rate of 2K/min under inert atmosphere (N_2 at 2l/min) and holding this temperature for a defined time span.

The trials included holding a temperature of 750°C for either 15, 30, 60, 180 or 300 minutes or 800°C for either 15, 60 or 180 minutes. These exact temperatures were chosen based on the results of the previous annealing trials (see chapter 5.4.2).
After annealing, the samples were impregnated as described in chapter 3.5.

3.4 Embedding and Infiltration

For microscopy and hardness measurements the powder and pieces of the compacted samples were embedded and additionally infiltrated in Struers EpoFix cold-curing epoxy resin. After a curing period of 24 hours the samples were ground with SiC sandpaper (22, 15, 10 and 8 µm) on a Struers Pedemin grinding machine and polished with diamond suspension (3 µm and 1 µm) on a Struers Tegramin grinding and polishing machine. The polished powder was etched using 3% Nital (3% HNO_3 in Methanol).

Unfortunately, this preparation method could not be applied to already impregnated samples (as described in 3.5). During the grinding, a majority of the particles would be removed from the surface and leave an enormous number of cavities. In a lot of cases the loose powder particles would additionally scratch the surface of the sample. Unlike the epoxy resin, the used Adhesive (Loctite 290) did not exhibit enough strength to hold the powder in place during grinding. For this reason, no microscopy investigations and therefore no microstructural results of the samples produced in the annealing trials can be presented, as the validity of any statement would be highly questionable.

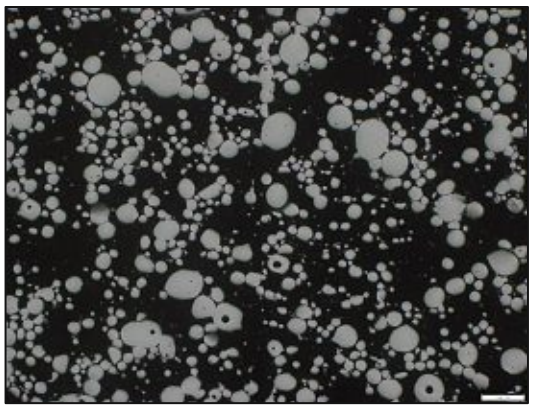

Figure 14 Ground and polished surface of a compacted sample, annealed at 800°C for 60min

3.5 Impregnation

Samples, that were produced with a paraffin content of 0.75% and a compaction pressure of 400 MPa, were impregnated after heat treatment to gain more stability.

For this purpose, an activator (Loctice SF 7649) was sprayed onto the samples and afterwards a threadlocking adhesive (Loctite 290) was applied. To ensure a thorough distribution of the adhesive the parts were additionally put under vacuum for one minute. For complete polymerisation of the adhesive a waiting duration of at least 24 hours was guaranteed.

Figure 15 shows that the described procedure leads to an even and thorough distribution of the adhesive throughout the sample.

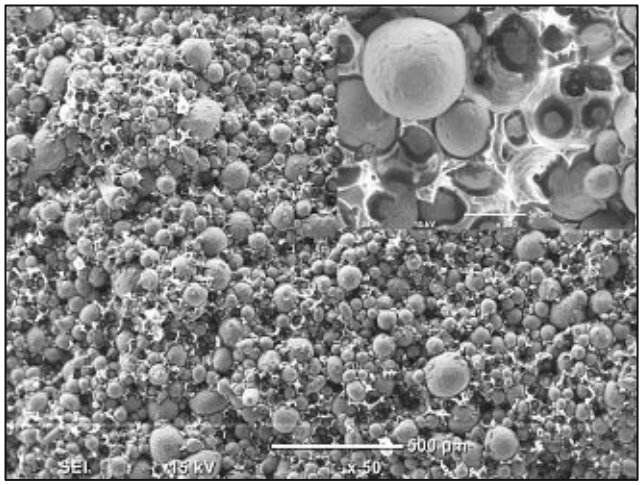

Figure 15 Fractured surface of an impregnated sample

4 Methods

4.1 Optical Microscopy

Optical Microscopy of the embedded samples, in polished and etched condition, was conducted with an Olympus GX51 Inverted Optical Microscope.

4.2 Scanning Electron Microscopy

Scanning Electron Microscopy was conducted on the loose powder as well as on the compacted samples. For this purpose, a FEI Quanta 200 Microscope and a Jeol JCM-6000 SEM were used.

4.3 X-Ray Fluorescence Analysis

To gain further information about the powder composition X-Ray Fluorescence Analysis (XRF) of the embedded powder, using an Axios wavelength XRF spectrometer with Rh Kα radiation, was conducted.

4.4 Particle Size Distribution

The particle size distribution (PSD) of the powder was determined by laser diffraction using a Sympatec Helos/BF particle size analyser combined with the Sympatec Vibri vibratory feeding unit and the Sympatec Rodos/M for dry dispersion of the powder sample.

4.5 Differential Thermal Analysis/Thermogravimetric Analysis (DTA/TG)

A DTA and TG measurement on the loose powder was conducted to gain a more detailed insight into the transformations during heating. For this purpose a Netzsch STA 449 F3 Jupiter thermal analyser was used to measure the DTA and TG curve between room temperature and 1000°C. Approximately 500 mg of the sample were placed in an Al_2O_3 crucible and temperature and mass difference measured while cooling and heating at a rate of 20K/min in argon atmosphere.

4.6 Density

The density of the compacted samples was determined by measuring the dimensions and mass of the samples and calculating the values.

ρ...Density [g/cm³]
m…Mass [g]
l...Length [cm]
w…Width [cm]
h…Height [cm]

$$\rho = \frac{m}{l \cdot w \cdot h} \qquad 11$$

4.7 Micro Hardness HVm)

The Vickers Hardness (HVm 0.1) was measured on all the samples during the pressing trials to see if a work hardening effect on the powder particles occur. It was measured using an Ahotec ecoHard XM1270 A hardness tester.

4.8 Electrical Resistivity

To determine the electrical resistivity the samples were mounted into the measurement setup shown in Figure 16 with a constant current of 1 A. With a multimeter the voltage drop of a sample was measured at four different distances, and the resulting resistivity was calculated.

Figure 16: Measurement setup for electrical resistivity

R…Resistance [Ω]
U_m…Measured voltage [V]
U_R…Reference voltage [V]
ρ…Specific resistivity [Ω·mm²·m⁻¹]
A…Cross sectional area of sample [mm²]
l…Distance between measuring points [m]

$$R = \frac{U_m \cdot 10\Omega}{U_R} \qquad 12$$

$$\rho = R \cdot \frac{A}{l} \qquad 13$$

4.9 Saturation Magnetisation and Coercivity

To determine the saturation magnetisation and coercivity of the samples a Foerster Koerzimat CS 1.096 was used.

4.10 Elemental Analysis

Elemental analysis of the carbon, oxygen and nitrogen content of the powder before and after a heat-treatment (600°C, 30 min) was conducted using a Leco CS230 Carbon/Sulfur Determinator (combustion analysis) and a Leco TC400-Nitrogen/Oxygen-Analyser (hot fusion analysis).

4.11 Attenuated-total Reflexion Infrared-Spectroscopy

To gain more information about the coating of the powder ATR-IR spectroscopy was conducted before and after heat-treatment (600°C, 30min) using a Spectrum 65 Perkin-Elmer FT-IR spectrometer with an ATR-crystal.

4.12 Transverse Rupture Strength

Transverse rupture strength was measured with a Zwick Roell universal testing machine in a 3-point bend setup with a support span of 30mm. TRS measurements were only conducted with samples pressed with a paraffin content of 0.75% at 400MPa after impregnation, as these were the only samples, that showed enough strength to yield useful results with this method.

4.13 X-Ray Photoelectron Spectroscopy

XPS measurements were conducted on the powder before and after a heat treatment at 600°C for one hour at inert atmosphere. to gain further insight on the nature of the powder coating. For these a SPECS XPS-spectrometer equipped with a monochromatised Al-Kα X-ray source (µFocus 350) and a hemispherical WAL-150 analyser (acceptance angle: 60°) was used. During measurement a pass energy of 100 eV and energy resolutions of 0.5 eV were used for survey and detail spectra (excitation energy: 1486.6 eV, beam energy and spot size: 70 W onto 400 x 400 µm², angle: 51° to sample surface normal, base pressure: 1 x 10^{-9} mbar).

For analysis of the spectra the software CASA XPS was used.

5 Results and Discussion

4.1 Fe-Si powder

Figure 17 and Figure 19 clearly show the uniformly round shape of the powder particles, in contrast to the irregular shape of the Somaloy 130i 5P powder (Figure 20). This spherical shape is likely one of the reasons for the poor compressibility of the Fe-Si powder. Some of the powder particles also show closed pores internally.

Figure 18 shows the etched profile of the powder particles.

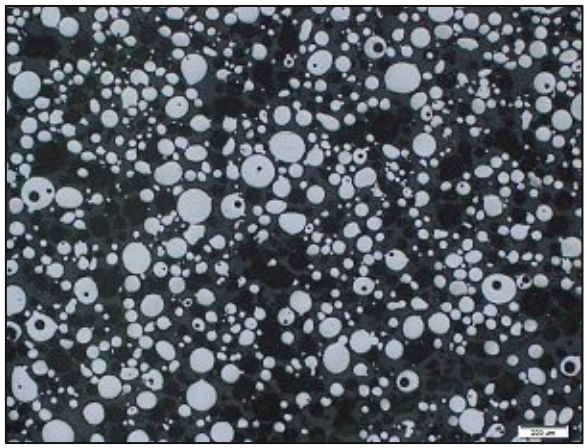

Figure 17: Section of Fe-Si powder after polishing

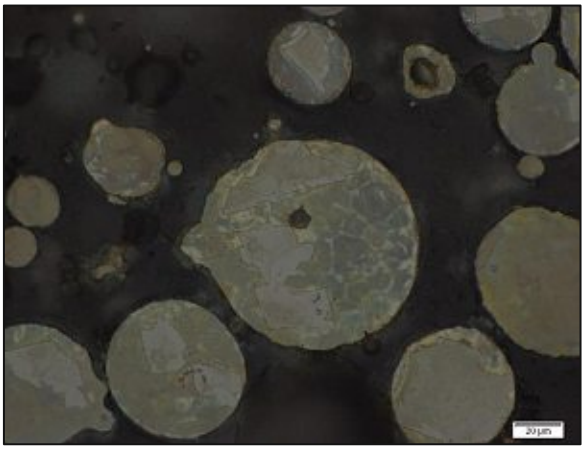

Figure 18: Fe-Si powder after polishing and etching

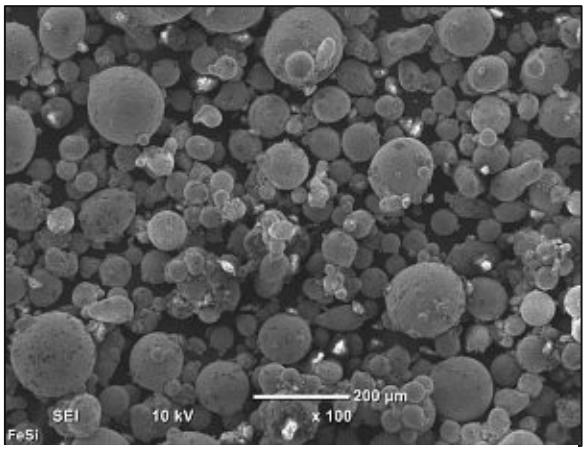

Figure 19: SEM picture of the Fe-Si powder

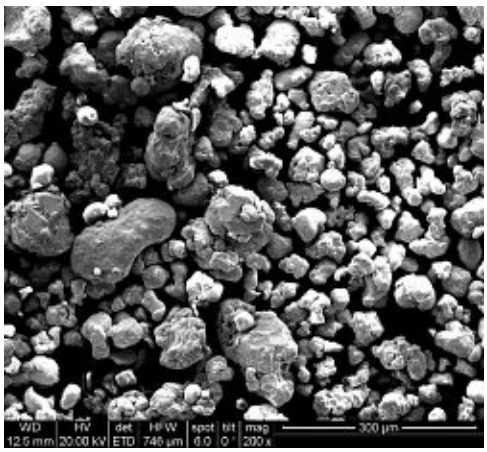

Figure 20 SEM picture of Somaloy 130i 5P powder, Höganäs [28]

5.1.1 Powder composition

Table 1 shows the results from the XRF and elemental analysis of the powder. It was found that the carbon content of the powder is significantly lower after a heat treatment (600°C, 30 min). Therefore, it can be assumed that the powder is coated with an organic layer, which degrades / evaporates at higher temperatures.

	XRF Analysis [%]	Elemental Analysis (before/after heat treatment) [%]	
Fe	96.47	-	-
Si	3.42	-	-
C	-	0.51	0.06
O	-	0.11	-
N	-	0.03	-
Ni	0.03	-	-
Cr	0.02	-	-
Cu	0.02	-	-
Mn	0.01	-	-
P	0.01	-	-
S	0.01	-	-
Mo	0.01	-	-

Table 1 XRF and elemental analysis of the powder

5.1.2 Attenuated Total Reflexion Infrared Spectroscopy

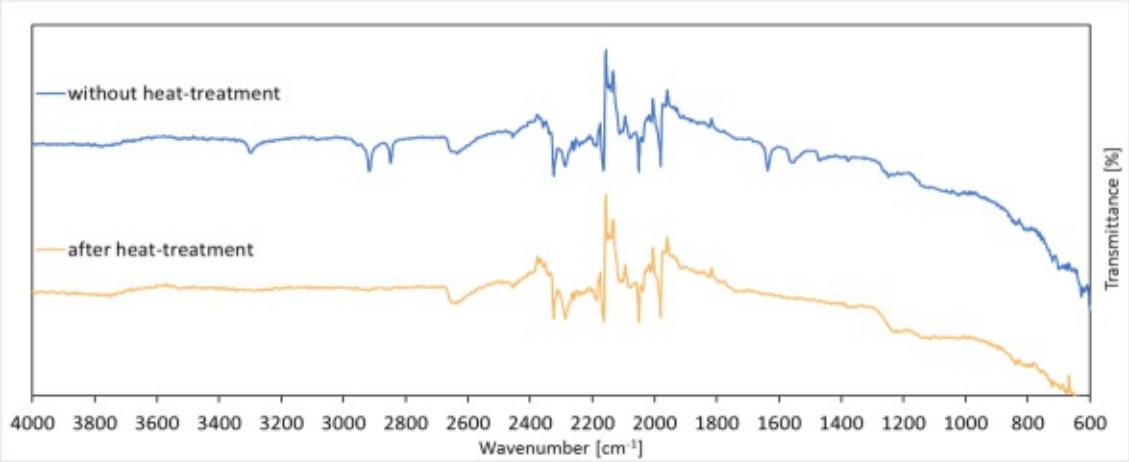

Figure 21: ATR-IR spectra of the powder before and after heat-treatment at 600°C

The ATR-IR spectrum of the Fe-Si powder (Figure 21) shows various peaks, relevant ones listed in Table 2. The signals between approximately 2600 cm^{-1} and 1800 cm^{-1} can be attributed to the IR spectrometer, so this area is unfortunately not useable for interpretation. The disappearance of the relevant peaks after a heat treatment also shows the disintegration of an organic layer at elevated temperatures. Without further information it is not possible to determine the exact structure of the organic compound on the particles. However, the spectrum indicates, that it might be a silane containing an alkene group.

Wavelength [cm^{-1}]	Possible Group
3298	O-H stretching (alcohol/carboxylic acid) N-H stretching
2917	C-H stretching (alkane)
2849	C-H stretching (alkane)
1636	C=C stretching (alkene) Si-CH2-CH2=CH2
1554	C=C (alkene)

Table 2 Possible functional groups of the measured peaks [29, 30]

5.1.3 Particle Size Distribution

The particle size distribution was measured three times and the yielded mean values for the cumulative size distribution at 10%, 50%, or 90% are listed in Table 3.

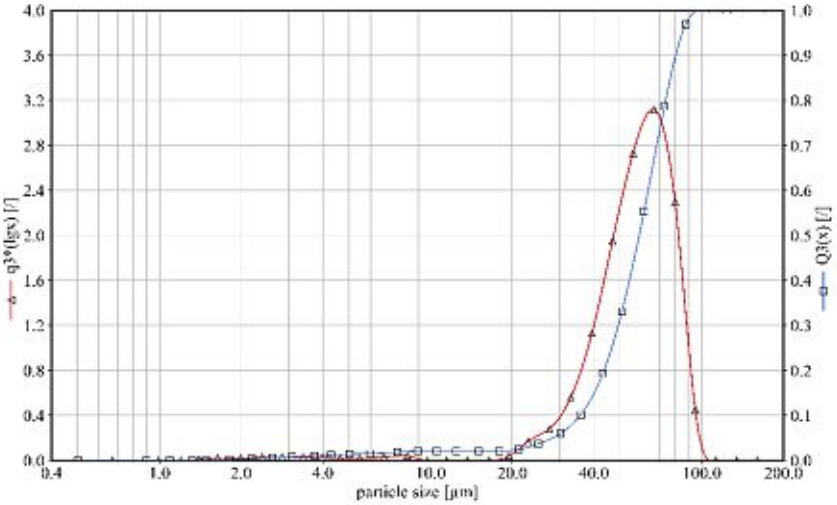

Figure 22: Example of a measured particle size distribution graph of the Fe-Si powder

D_{10}	D_{50}	D_{90}
31 ± 4 µm	56 ± 3 µm	77 ± 6 µm

Table 3 Particle size distribution of the FeSi powder

5.1.4 X-Ray Photoelectron Spectroscopy

Qualitative and quantitative analysis of the XPS spectra was conducted. The results of the quantitative analysis have to be treated with caution, as it is not known how thick the coating on the powder is and how far the radiation penetrates through the layer into the bulk of the particles. Still, the quantitative results give a rough overview of the element ratios.

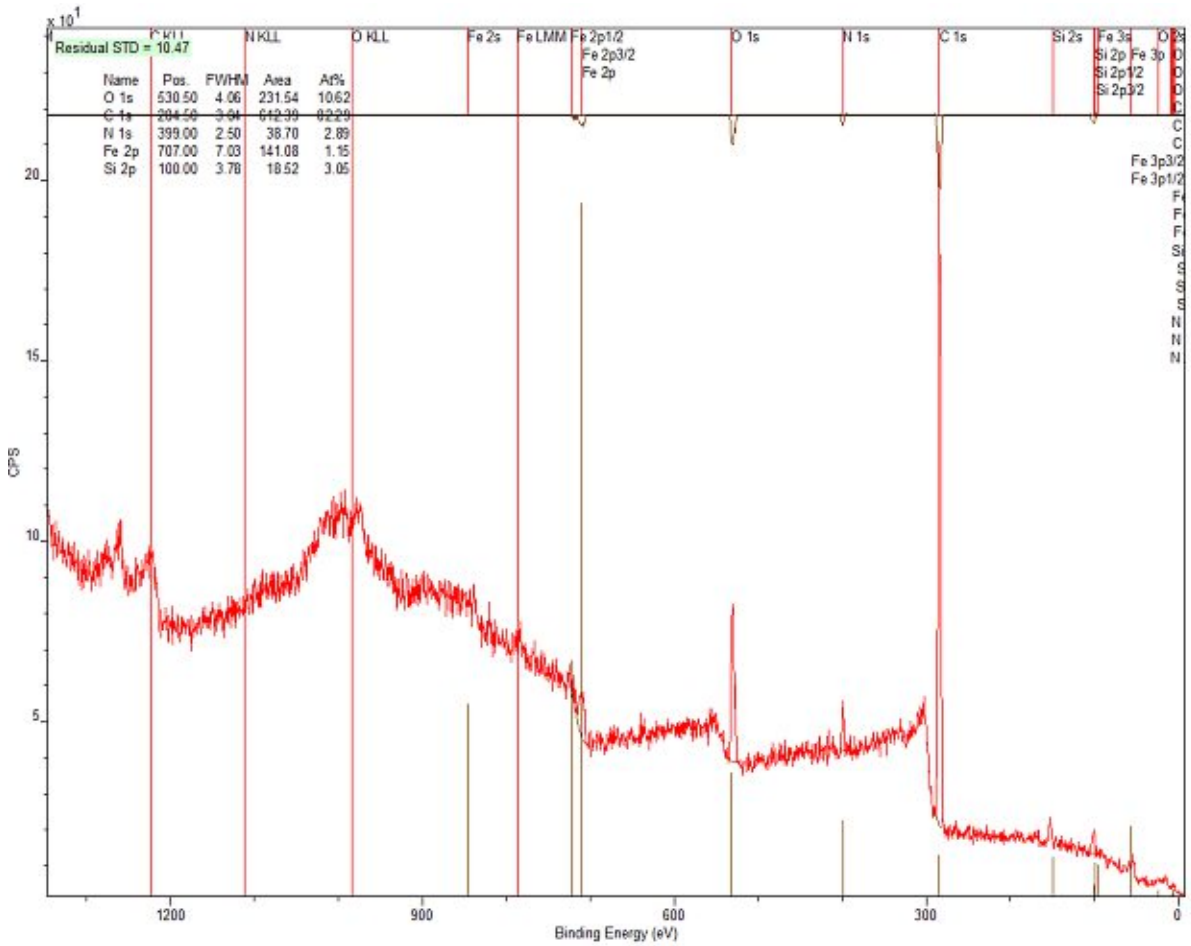

Figure 23: Survey spectrum of the FeSi powder

Element	Amount before heat treatment [at%]	Amount after heat treatment (600°C, 1 hour) [at%]
C	82.29	51.41
N	2.89	4.52
O	10.62	27.60
Fe	1.15	3.46
Si	3.05	11.35

Table 4: Quantitative analysis of the XPS survey spectra before and after heat treatment

The XPS survey spectrum of the powder without sputtering showed a carbon content of approximately 82%, while the heat-treated powder only showed 51%. This, and the earlier shown ATR-IR spectrum, proof, that the powder owns an organic coating that disintegrates at elevated temperatures. Figure 26 shows the detail spectrum of the carbon peak. For fitting C-C, C-H and C-O components were taken into consideration, as suggested by the ATR-IR spectrum, as well as a C-Si part, in respect to the XPS detail spectrum of the silicon peak (see below). The spectra from the XPS and ATR-IR (see chapter 5.1.2) suggest that the organic layer on the powder could be a kind of silane, as there has to be silicon present in the organic structure and there seems to be no indicator for a conjugated carbon structure. However, the exact structure of the organic layer still cannot be identified from the collected data.

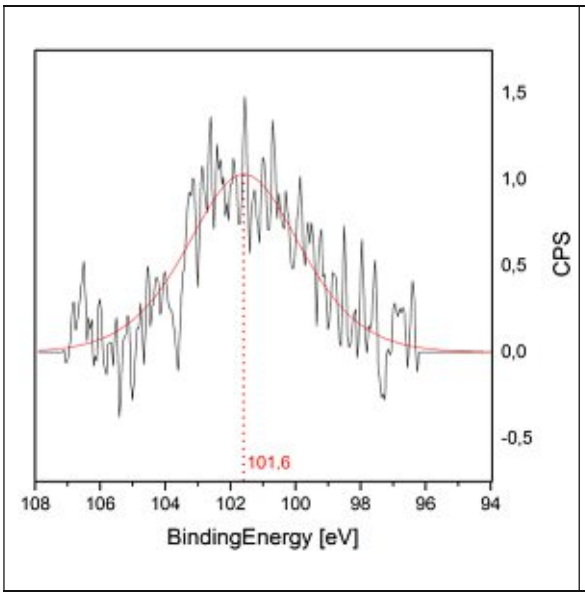

Figure 24: XPS detail spectrum of silicon before heat treatment

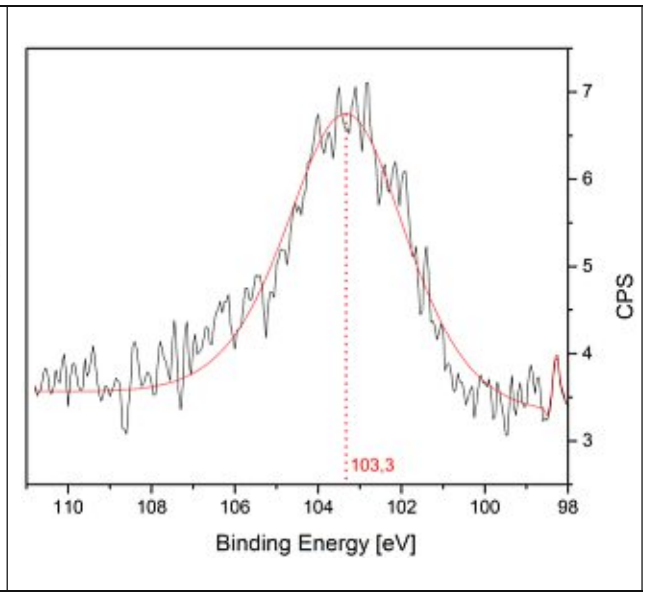

Figure 25: XPS detail spectrum of silicon after heat treatment at 600°C

The detail spectra of silicon (Figure 24 and Figure 25) show a shift in the binding energy before and after heat treatment from 101.6, which is typical for organic silicon, to 103.3., which is most probably SiO_2 [31],[32]. This means that only through a heat treatment an insulating coating of SiO_2 forms. SiO_2 coated iron-based SMC powders show some disadvantages, because they are easily damaged during compaction or heat treatment due to their brittleness [33]. Additionally, the discrepancy in the thermal expansion coefficients possibly decreases the stability of the coating even further. The lower CTE for SiO_2 ($5*10^{-7}°K^{-1}$ [34] compared to iron at $11.8*10^{-6}°K^{-1}$ [35]) might create even more strain on the material. By building up a SiO_2 coating at the final annealing step, the mentioned problems can be avoided.

Figure 27 shows the detail spectrum of the iron peak. Apparently, the surface of the powder also exhibits a layer of iron oxides on the surface, which is not surprising as iron tends to oxidise rather easily. Identification of the iron oxides was attempted, still a precise fitting of these spectra is difficult, as iron oxides show a variety of peaks at similar binding energies [36].

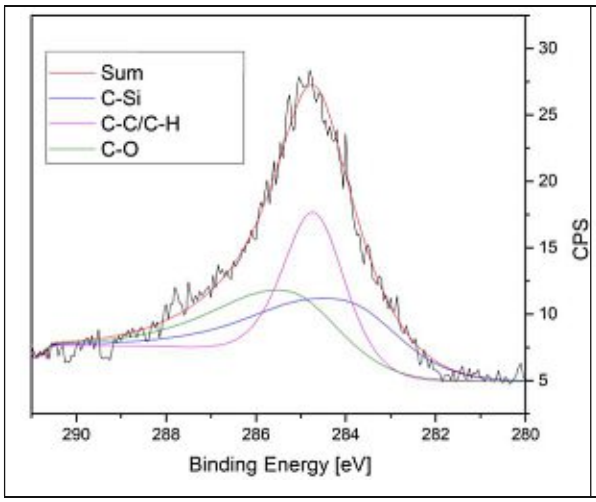

Figure 26 Detail XPS spectra of the carbon peak

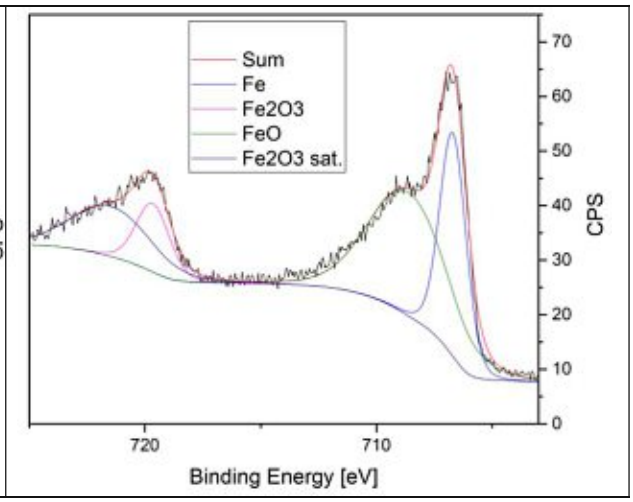

Figure 27: Detail XPS spectrum of the iron peak

In conclusion, the results of the XPS suggest the transformation of an organic layer on the powder to a SiO_2 coating. Furthermore, the existence of a layer of iron oxides was proofed. Figure 28 vaguely illustrates the proposed transformation of the powder.

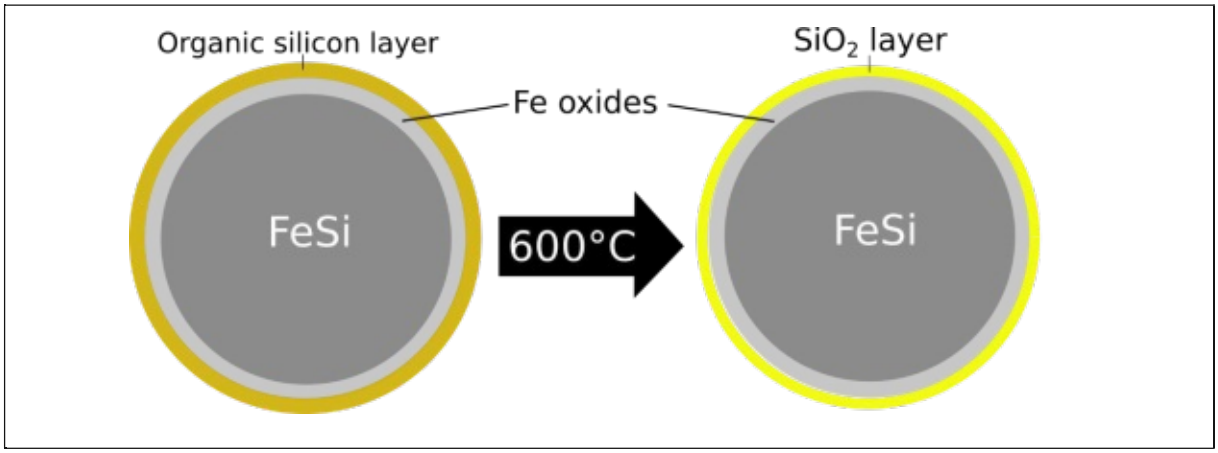

Figure 28 Proposed mechanism of the effect of the annealing treatment on the powder

5.1.5 Differential Thermal Analysis/Thermogravimetric Analysis

The TG curve (Figure 29) shows a weight loss of the powder of approximately 0.60%, which can be attributed to two different appearing effects which are revealed by the DTG curve at 373.1°C and 452.1°C. An explanation for this could be the disintegration of an organic silicon layer consisting of two steps, for instance an oxidation including a rearrangement of the structure.

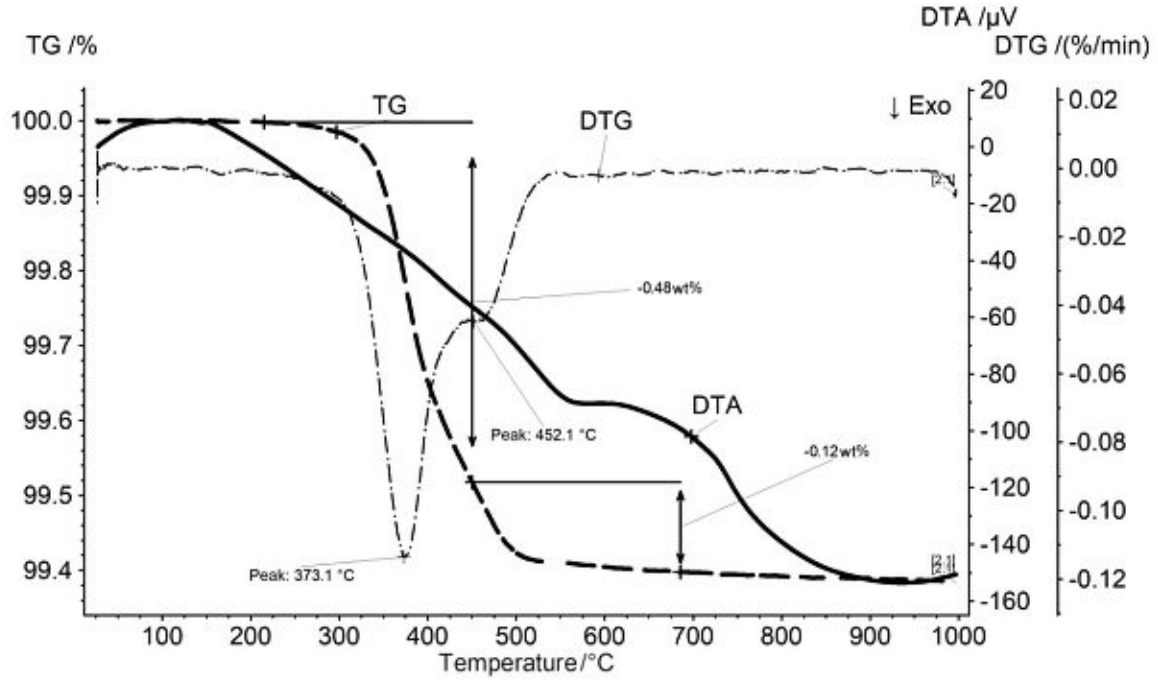

Figure 29 DTA and TG/DTG curve of the FeSi powder

The DTA curve also shows effects between 600°C and 800°C. The DDTA (Figure 30) curve suggests, that at least two different effects overlap here. The formation of an SiO_2-layer probably takes place in this region, as also suggested by the increasing electric resistivity of the compacted samples at 700°C. Other occurring effects could be caused by the oxidation of iron or a magnetic transition of the alloy.

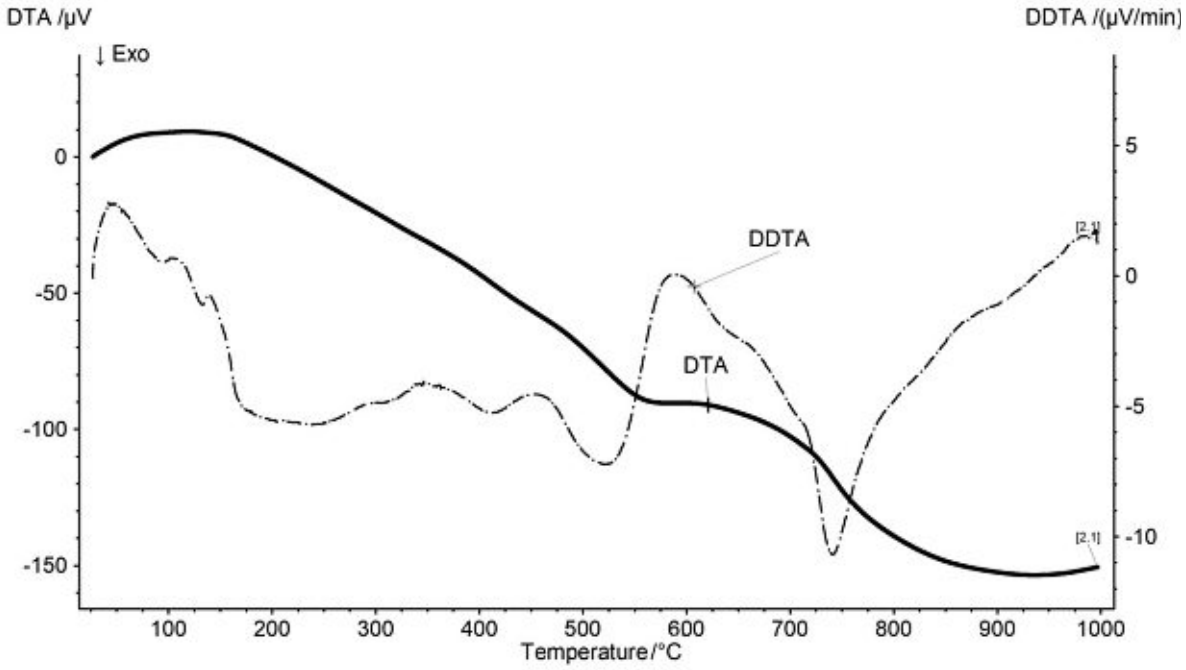

Figure 30 DTA and DDTA curve of the FeSi powder

5.2 Density

5.2.1 Pressing Trials

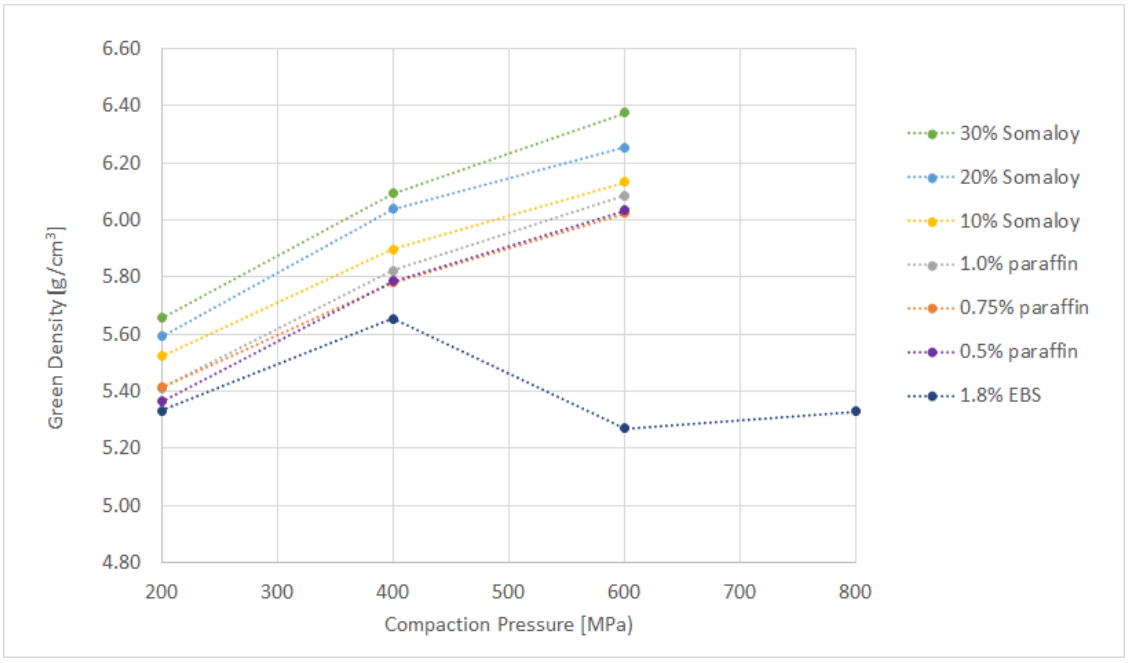

Figure 31: Density values of the green samples with increasing compaction pressure

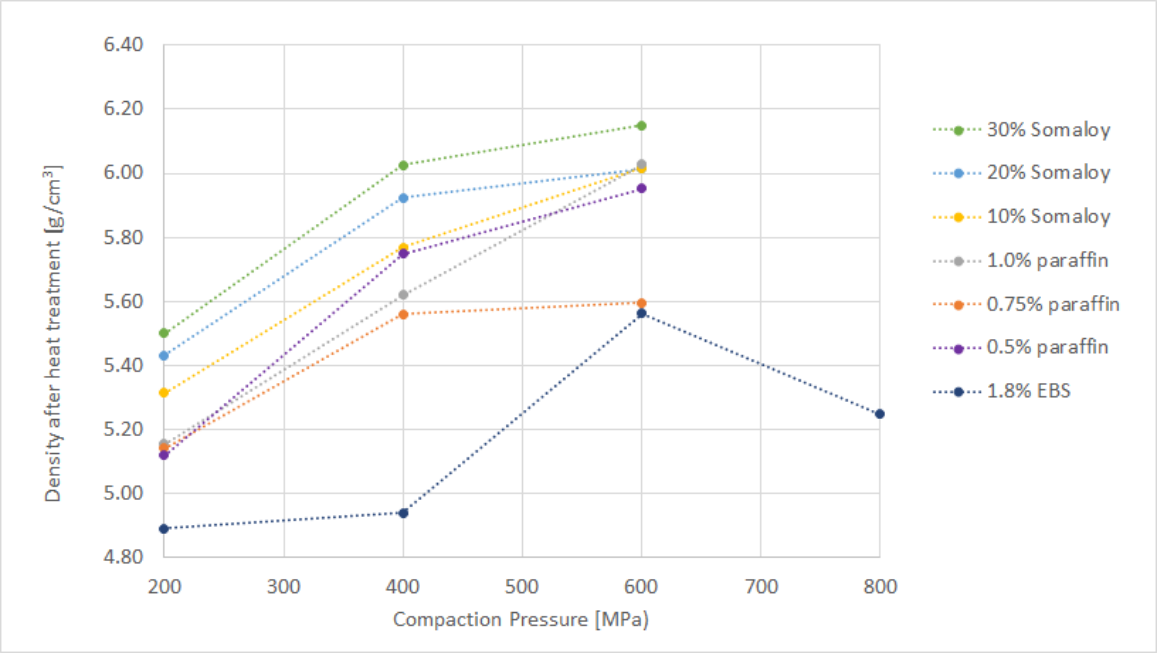

Figure 32: Density values of the samples after heat treatment with increasing compaction pressure

Figure 31, Figure 32 and Table 5 show the density values of the single specimens. The values generally increase with higher pressures, as typical for compaction of metal powders. The only exceptions seem to be samples of the 1.8% EBS-series pressed at 600 and 800 MPa. The reason for this surprising behaviour is the high hardness and the spherical shape of the powder, which causes a springback effect while relieving the pressure after compacting. Furthermore, the sample showed cracks instantly after pressing, which made the determination of the dimensions unprecise. Even though samples compacted at 600 MPa showed the highest densities, further experiments were conducted mainly at 400 MPa, because specimens thus compacted showed the highest stability and had a lower tendency to break or crack.

	Pressing aid [wt%]	Somaloy 130i 5P [wt%]	Compaction pressure [MPa]	Green density [g/cm³]	Density after annealing [g/cm³]
EBS	1.8	-	200	5.33	4.89
			400	5.65	4.94
			600	5.27	5.56
			800	5.33	5.25
Paraffin	0.5	-	200	5.36	5.12
			400	5.78	5.75
			600	6.03	5.95
	0.75	-	200	5.41	5.14
			400	5.78	5.56
			600	6.02	5.60
	1.0	-	200	5.41	5.15
			400	5.82	5.62
			600	6.09	6.03
EBS	1.0	10	200	5.52	5.31
			400	5.90	5.77
			600	6.13	6.02
		20	200	5.59	5.43
			400	6.04	5.92
			600	6.25	6.01
		30	200	5.66	5.50
			400	6.09	6.03
			600	6.38	6.15

Table 5: Single density values of the compacted samples

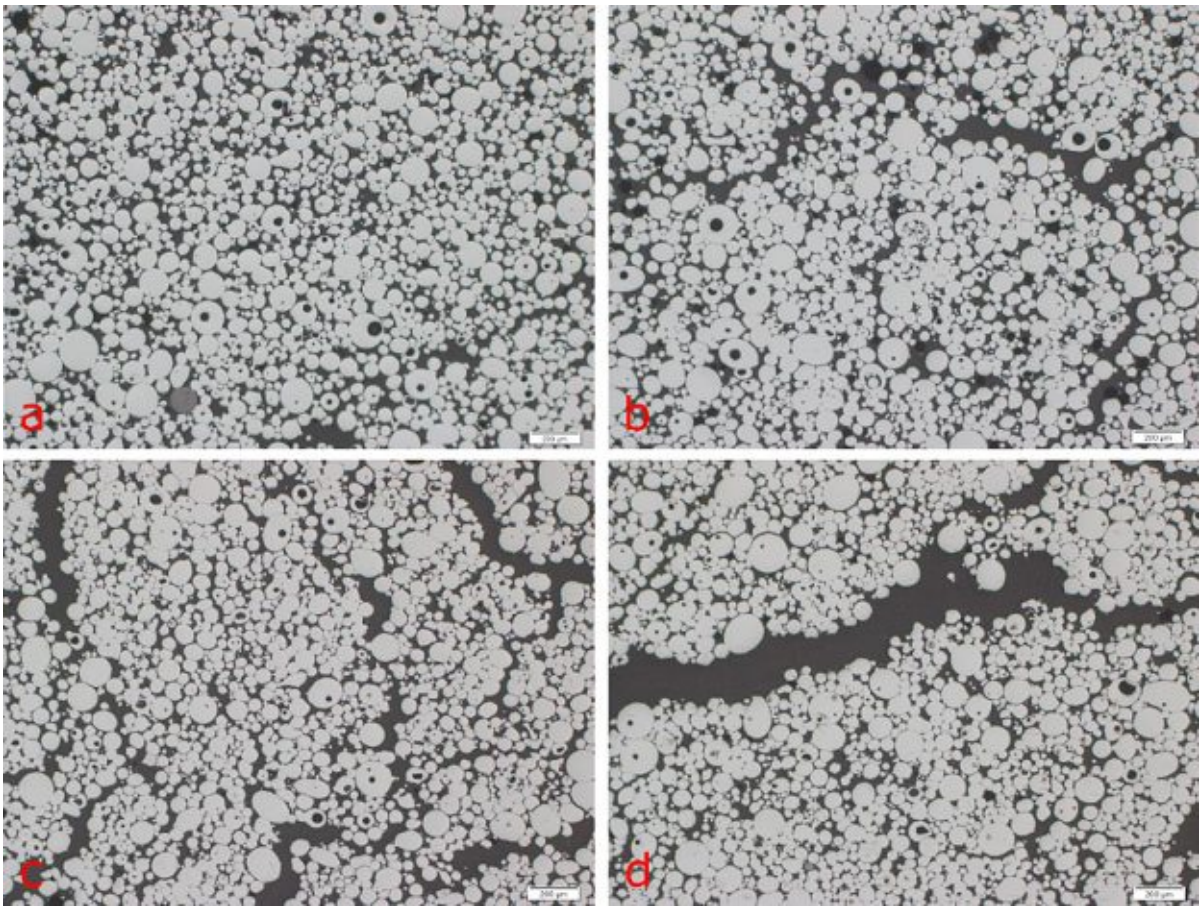

Figure 33: Polished samples compacted with 1.8% EBS at 200 MPa (a), 400 MPa (b), 600 MPa (c) and 800 MPa (d)

Figure 33 shows clearly how the samples of the 1.8% EBS-series densify with increasing pressure, but also how more and bigger cracks occur.

The paraffin samples did not develop cracks at compaction compared to the samples pressed with 1.8% EBS (see Figure 34). The homogeneous distribution of the pressing lubricant through dissolving in cyclohexane might lead to less strain during compaction and therefore prevent cracking. Samples pressed at 600 MPa unfortunately still exhibited very low stability and were damaged easily during preparation. Therefore, it seemed reasonable to conduct the following annealing experiments at a compaction pressure of 400 MPa. For paraffin addition, 0.75% was chosen, as it was a sufficient amount to produce stable samples.

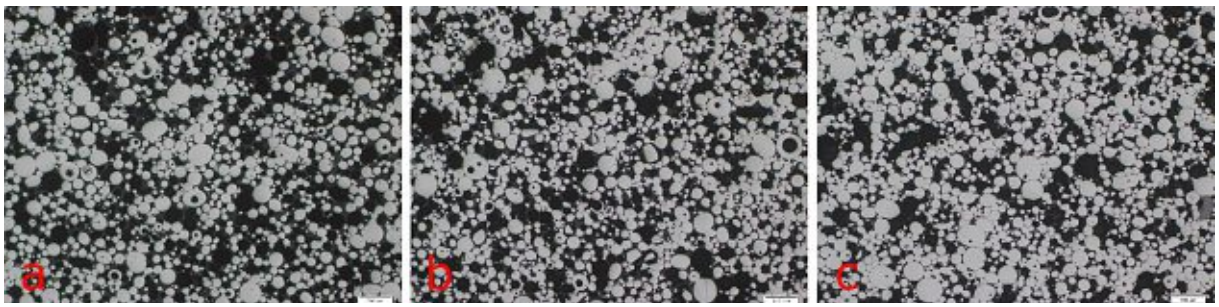

Figure 34: Samples compacted with 0.75% paraffin at 200 MPa (a), 400 MPa (b) and 600 MPa (c)

The samples consisting of both Fe-Si and Somaloy powder reach the highest densities. Figure 35 depicts how the irregular particles of the Somaloy powder form dense areas throughout the sample and therefore increase the density in general. This clearly shows the influence of the powder shape and hardness on the samples' performance and how the irregular shape of the Somaloy powder is better suited for compaction than the Fe-Si powder supplied by the partner.

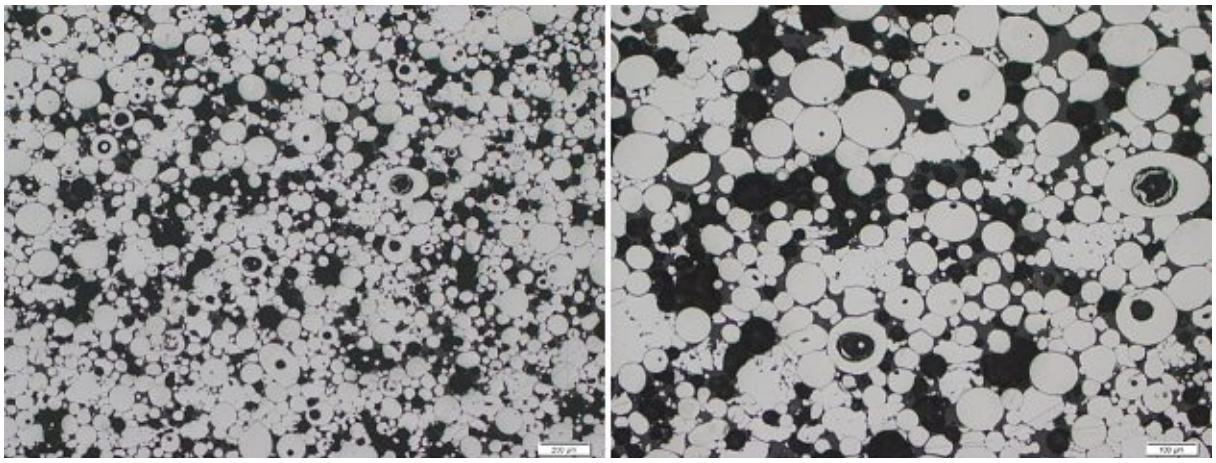

Figure 35: Sample with 20% Somaloy compacted at 600 MPa

5.2.2 Annealing Trials

As the samples for the annealing trials were consequently compacted at 400 MPa with a paraffin addition of 0.75% only densities between 5.78 – 5.92 g/cm^3 were measured, resulting in a mean value of 5.86 g/cm^3 with a standard deviation of 0.03.

5.3 Hardness

The hardness of the compacted samples is in most cases slightly higher than in the loose powder (see Figure 36). This might be caused by work hardening effects on the powder during compaction [37]. However, the values show relatively large standard deviations (see Table 6)

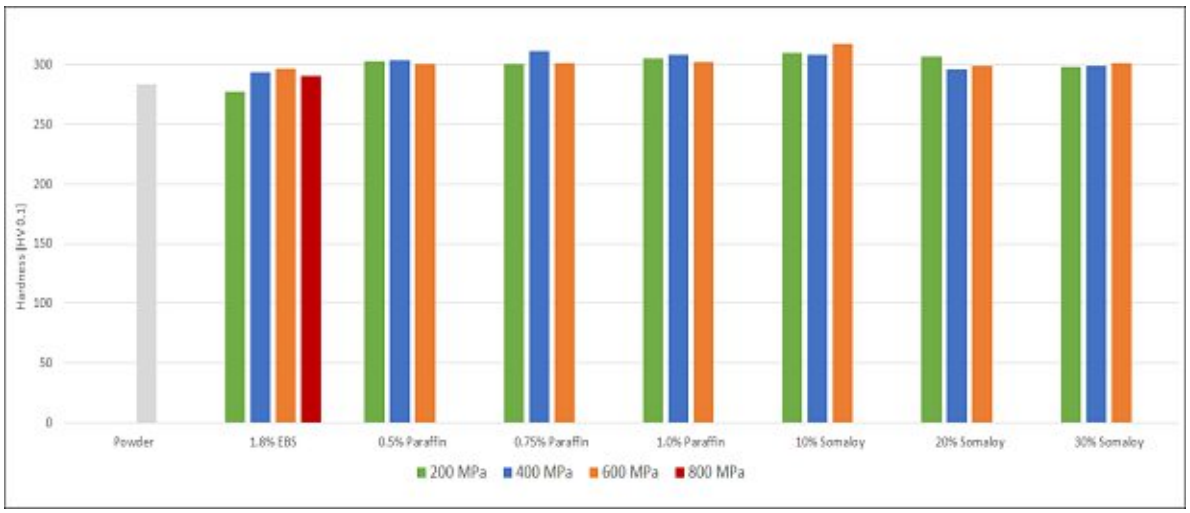

Figure 36: Vickers Microhardness of the samples

so it is not certain if compaction has a significant effect on the hardness of the powder particles. In any case, the high hardness of the Fe-Si powder is shown, which is not surprising since Si has a very pronounced solid solution strengthening effect on ferrite, even more so than Mn [3].

	Pressing aid [wt%]	Somaloy 130i 5P [wt%]	Compaction pressure [MPa]	Hardness [HV 0.1]	Standard Deviation [HV 0.1]
Fe-Si powder	-	-	-	283	10
EBS	1.8		200	277	16
			400	294	14
			600	296	17
			800	290	15
Paraffin	0.5		200	303	9
			400	304	12
			600	300	33
	0.75		200	300	10
			400	311	16
			600	301	31
	1.0		200	305	15
			400	308	11
			600	302	18
EBS	1.0	10	200	310	11
			400	308	11
			600	317	9
	1.0	20	200	307	14
			400	296	18
			600	299	16
	1.0	30	200	298	11
			400	299	13
			600	301	13

Table 6: Vickers hardness values of the FeSi powder and the compacted samples

5.4 Electrical and magnetic properties

5.4.1 Pressing Trials

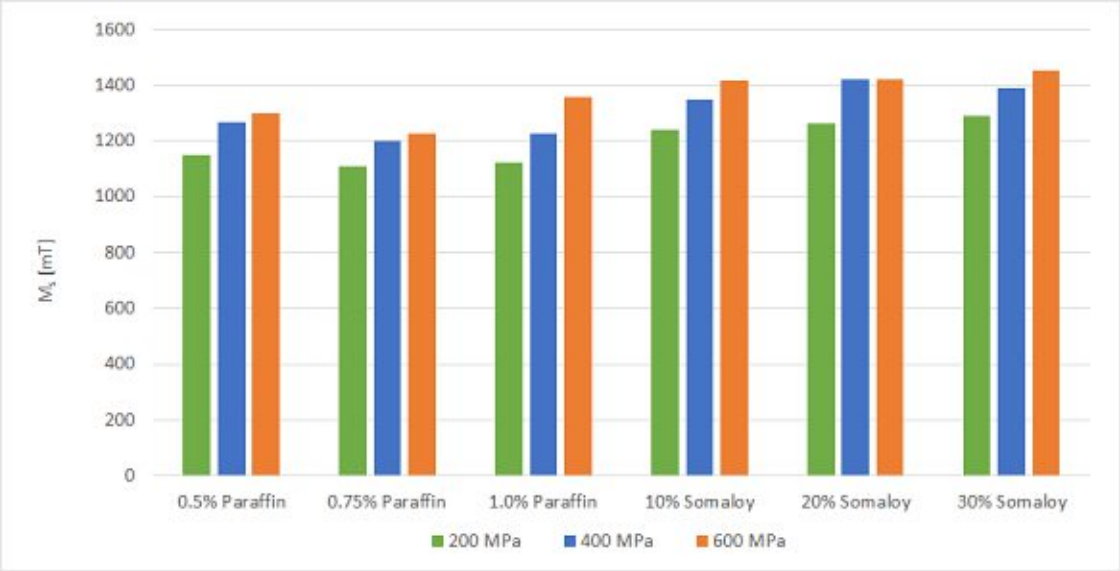

Figure 37: Saturation magnetisation M_s

The volume specific saturation magnetisation M_s (Figure 37) increases with higher compaction pressure. As already shown in chapter 5.2.1 the density increases with higher compaction pressure, hence the saturation magnetisation is higher when the sample is denser and thus contains more ferromagnetic volume.

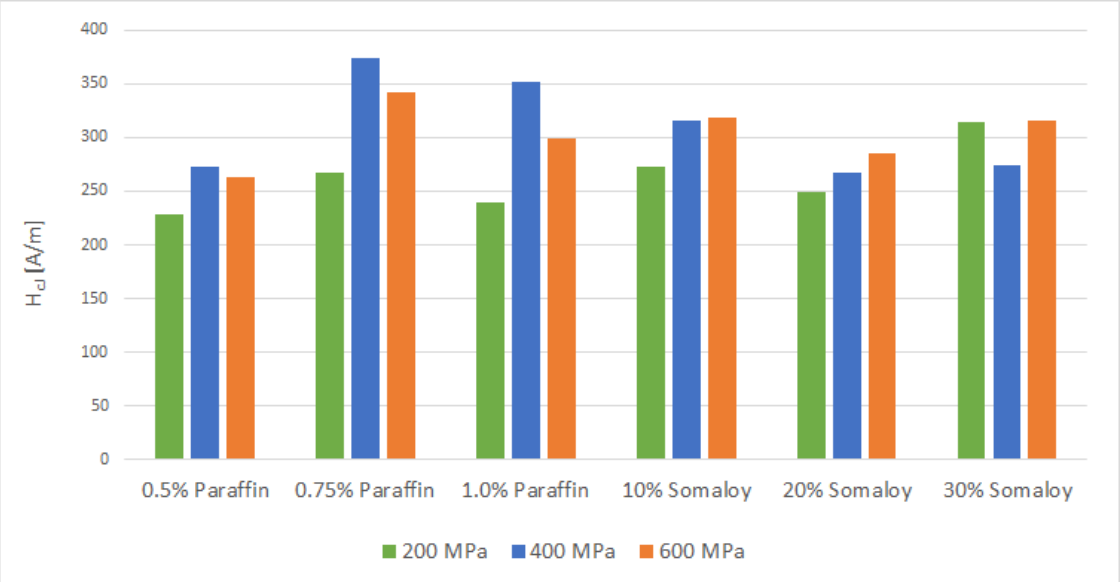

Figure 38: Coercivity H_{cJ}

The coercivity H_{cJ} (Figure 38) seems to be lowest at a compaction pressure of 200 MPa, which indicates that it might increase in general with higher pressures. A decrease in coercivity can be observed in samples pressed with paraffin at a pressure of 600 MPa, while in the case of

the Somaloy samples it increases, possibly because of higher dislocation density in these soft and therefore well compactible powders [23].

	Addition [wt%]	Compaction pressure [MPa]	Volume specific saturation magnetisation M_S [mT]	Standard deviation [mT]	Coercivity H_{CJ} [A/m]	Standard deviation [A/m]
Paraffin	0.5	200	1149	3.7	229	19.8
		400	1267	2.0	273	30.4
		600	1299	3.4	263	24.9
	0.75	200	1110	1.2	268	11.4
		400	1201	9.5	374	6.8
		600	1224	3.0	342	9.8
	1.0	200	1122	4.3	240	12.6
		400	1225	7.0	352	12.1
		600	1356	3.1	299	20.1
Somaloy 130i 5P	10	200	1240	0.9	273	35.2
		400	1349	3.5	315	39.6
		600	1416	4.6	319	59.0
	20	200	1263	2.2	249	50.6
		400	1419	1.6	268	43.3
		600	1418	2.8	285	12.9
	30	200	1291	6.9	315	17.2
		400	1390	5.4	275	132.7
		600	1452	5.4	316	21.4

Table 7: Magnetic properties of the compacted samples

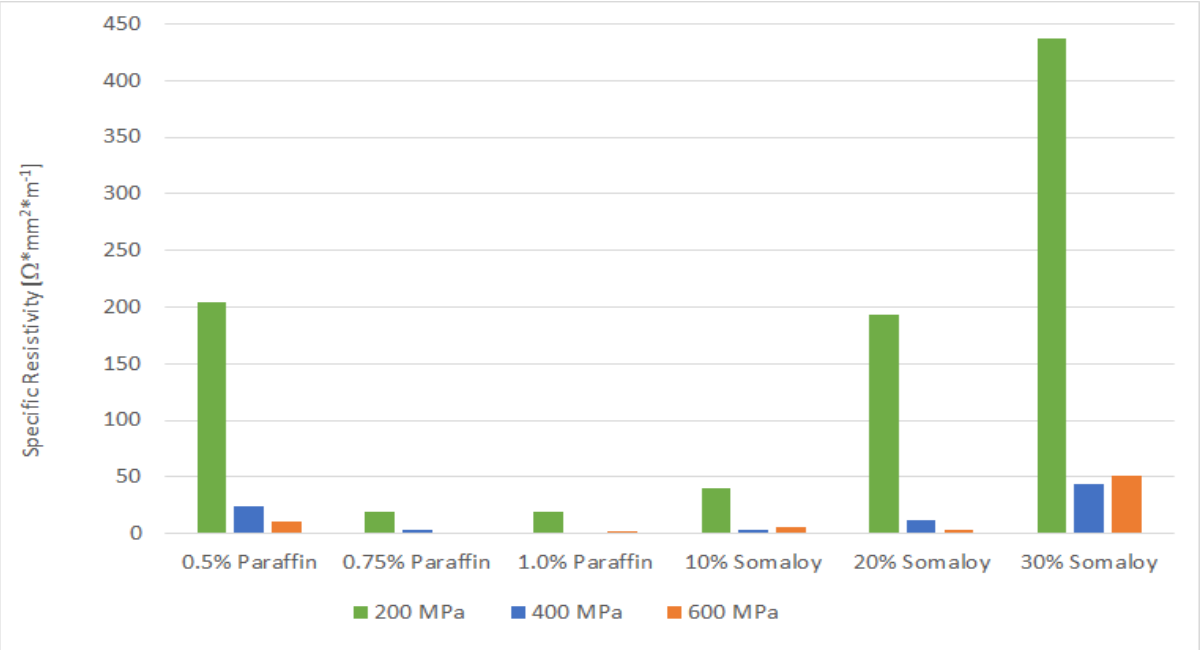

Figure 39: Specific resistivity of the samples

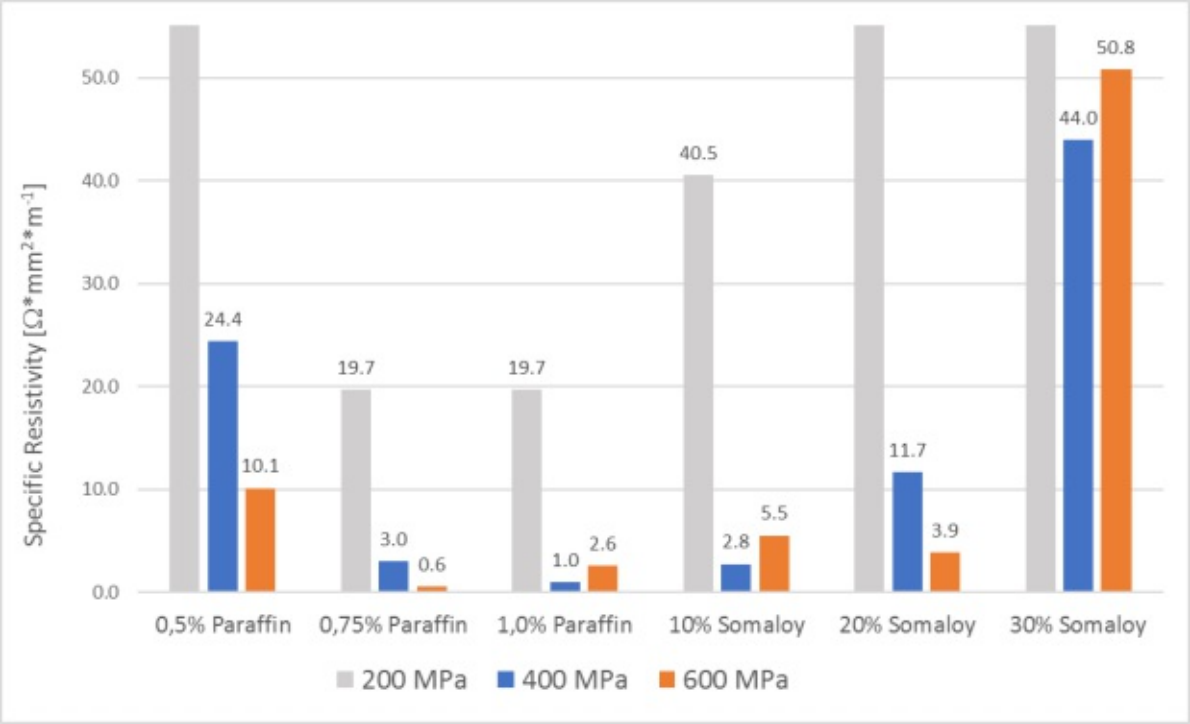

Figure 40: Specific Resistivity of the samples (readjusted Y-axis, see Figure 39)

The specific resistivity of the samples are presented in Figure 39 and Figure 40, where both charts show the same results, but with different axis intercepts to better depict the influence of the compaction pressure at 400 and 600 MPa. The values for the specific resistivity mostly decrease with higher compaction pressures. This behaviour can be explained by the decrease of porosity with higher pressure. The samples pressed with 0.5% paraffin at 200 MPa show noticeably higher resistivities than the samples pressed with a higher paraffin content. The reason for this behaviour is unfortunately not evident. The addition of Somaloy powder increases the resistivity of the samples. It can be assumed that the insulating coating of the Somaloy powder is more efficient compared to the Fe-Si powder at an annealing temperature of 600°C.

	Addition [wt%]	Compaction pressure [MPa]	Specific Electric resistivity [Ω*mm²*m⁻¹]	Standard deviation [Ω*mm²*m⁻¹]
Paraffin	0.5	200	203.9	109.2
		400	312.5	24.4
		600	184.5	10.1
	0.75	200	19.7	2.9
		400	7.4	3.0
		600	4.7	0.6
	1.0	200	19.7	0.4
		400	15.0	1.0
		600	64.1	2.6
Somaloy 130i 5P	10	200	40.5	3.5
		400	43.3	2.8
		600	44.7	5.5
	20	200	193.8	40.6
		400	86.9	11.7
		600	117.0	3.9
	30	200	436.7	77.9
		400	91.1	44.0
		600	357.1	50.8

Table 8: Specific electrical resistivity of the compacted samples

5.4.2 Annealing Trials

5.4.2.1 Annealing Temperature

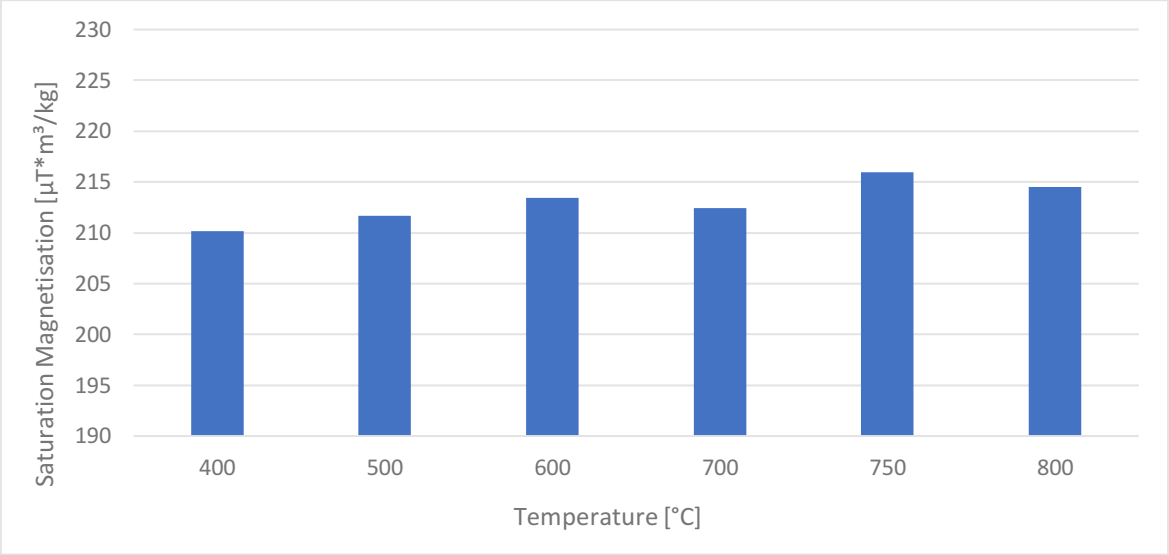

Figure 41: Saturation magnetisation at different annealing temperatures

As can be clearly seen in Figure 41 the saturation magnetisation does not show any significant changes with variation of annealing temperature.

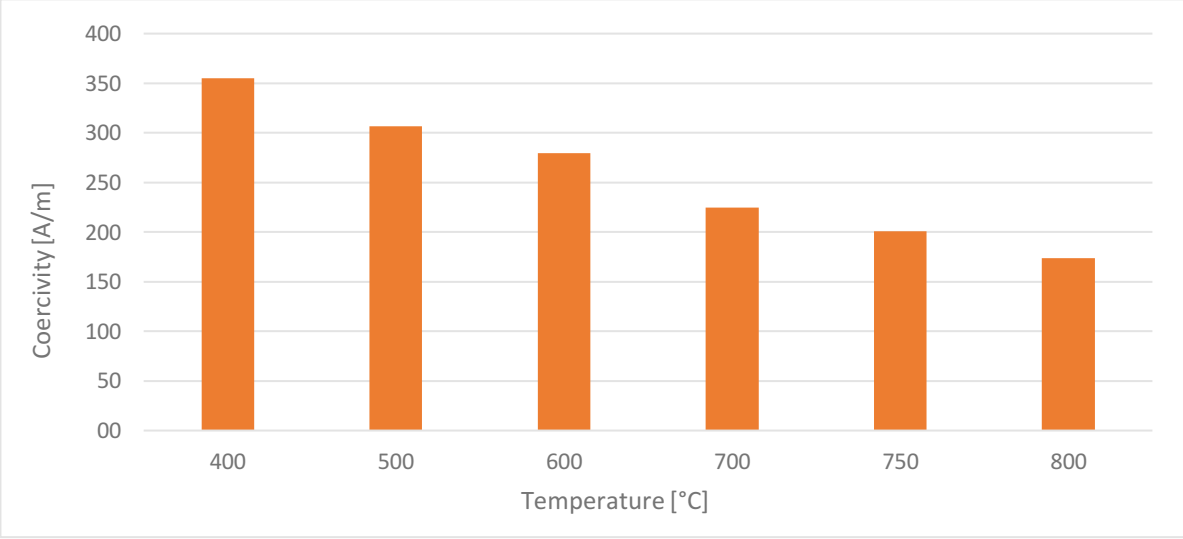

Figure 42 Coercivity at different temperatures

Figure 42 shows the decrease of coercivity with rising annealing temperatures. The compaction process induces microstrains on the material, which leads to higher coercivity. Longer annealing treatments or higher temperatures can relieve the induced stress and therefore lower the coercivity [23].

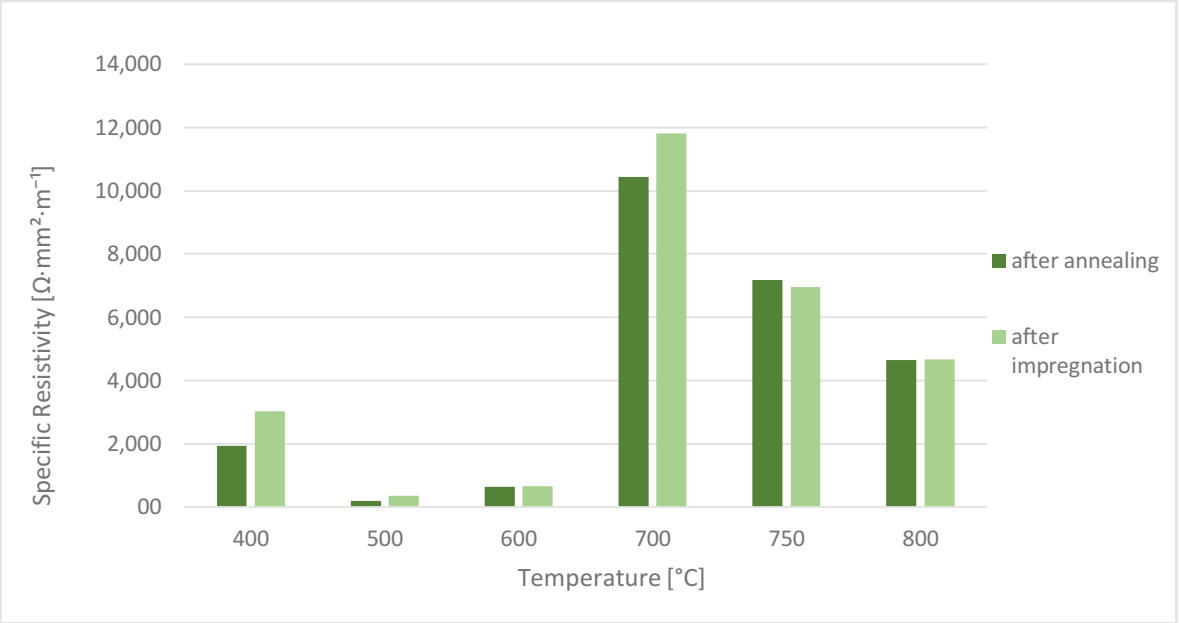

Figure 43 Specific resistivity of the samples at different temperatures

The specific resistivity of the samples shows a sharp increase at 700°C, followed by a gradual decrease at rising temperatures.

As already suggested by XPS measurements (see chapter 5.1.4) a SiO_2 layer on the particle surfaces starts to develop during annealing. The variation of annealing temperature shows that this process rapidly increases at or slightly below 700°C. At higher temperatures the resistivity declines. This can be explained by sintering processes, which start to degrade the insulating layer (as described in chapter 2.5.1).

Based on the received results for coercivity and specific resistivity, two temperatures, that offered an acceptable trade-off (750°C and 800°C) were chosen and different annealing durations at these temperatures evaluated.

5.4.2.2 Annealing duration

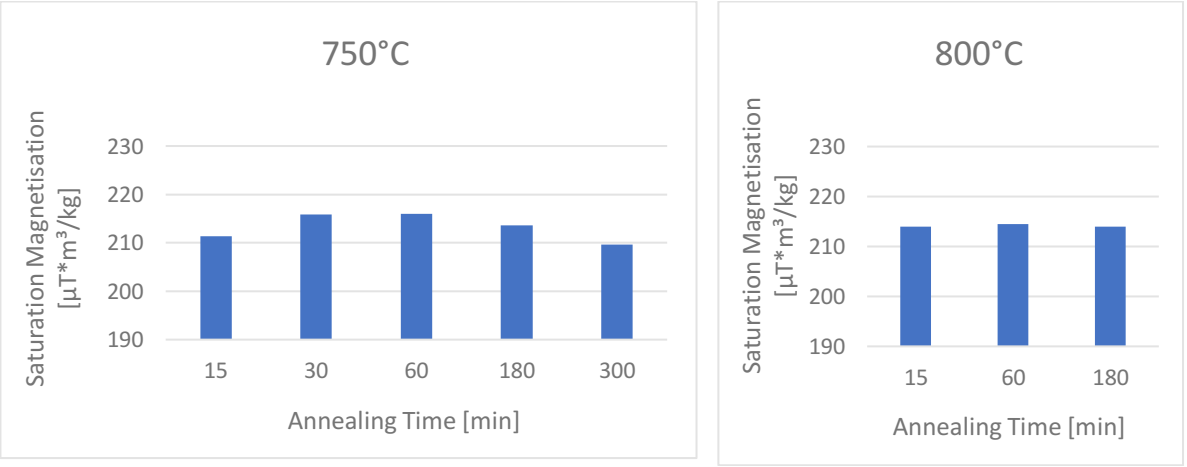

Figure 44 Saturation magnetisation at different annealing durations at 750°C and 800°C

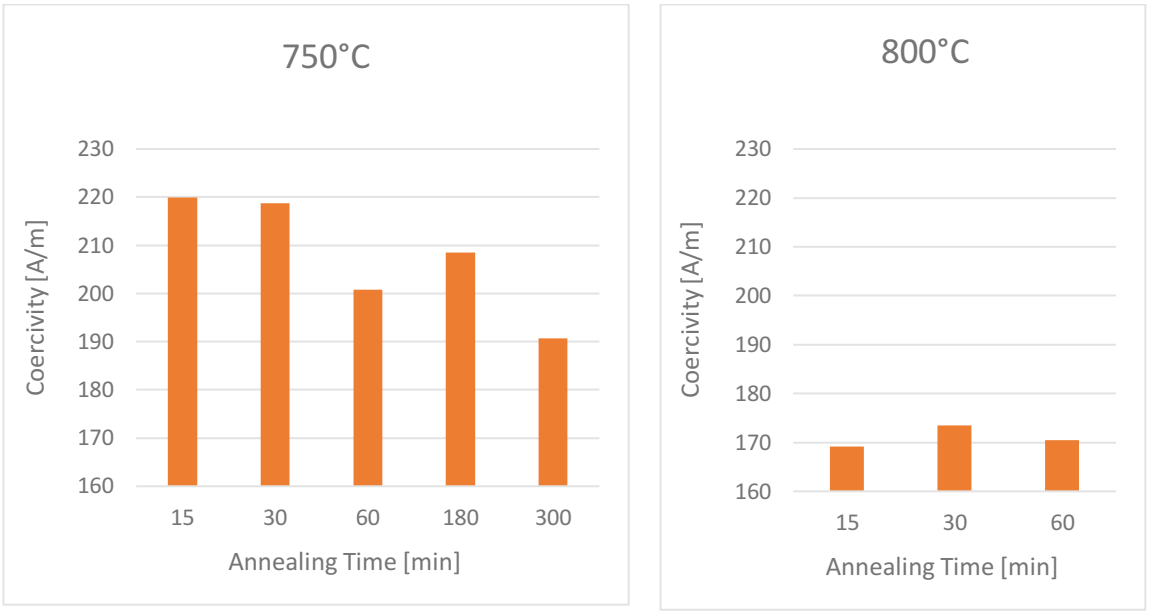

Figure 45: Coercivity values at different annealing durations at 750°C and 800°C

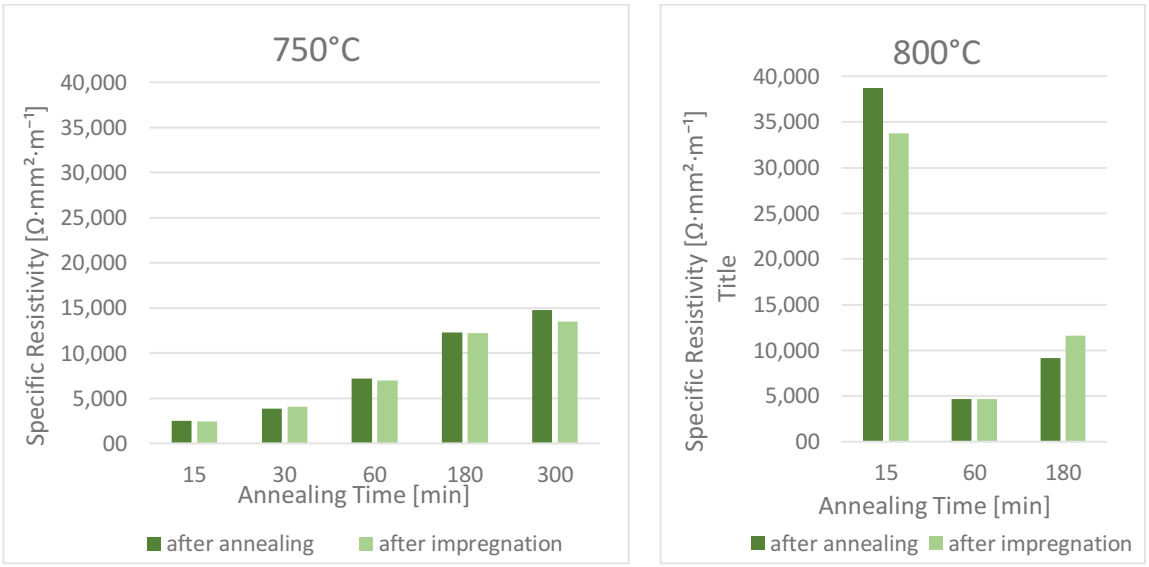

Figure 46: Specific resistivity of the samples at different annealing durations at 750°C and 800°C

The duration of the annealing treatment, as well as the temperature, does not influence the saturation magnetisation (see Figure 44). Therefore, it is almost certain, that improvement of these values can only be achieved by increasing the density of the parts.

At 750°C annealing temperature the properties of the samples reach their best performance at an annealing duration of 300 minutes, providing a coercivity of 191 A/m and a specific resistivity of 14.788 $\Omega \cdot mm^2 \cdot m^{-1}$ (see Figure 45 and Figure 46). This temperature is low enough to avoid sintering of the powder, therefore longer periods of heating continuously enhance the electromagnetic properties.

At 800°C the coercivity is not noticeably affected by changes of the annealing duration. Apparently, this temperature is high enough to allow for complete stress-relief of the material.

The specific resistivity at this annealing temperature reaches its highest value (38.674 $\Omega \cdot mm^2 \cdot m^{-1}$) after 15 minutes, which again rapidly declines at longer durations (see Figure 46). This decline of the resistivity is probably caused by the aforementioned sintering.

Annealing Temperature [°C]	Annealing Duration [min]	Coercivity [A/m]	Specific Resistivity (after impregnation) [$\Omega \cdot mm^2 \cdot m^{-1}$]
400	60	355	3035
500	60	307	348
600	60	280	656
700	60	225	11809
	15	220	2423
	30	219	4051
750	60	201	6957
	180	209	12185
	300	191	13513
	15	169	33773
800	30	173	4669
	60	170	11609

Table 9 Coercivity and specific resistivity values of annealing trials

In conclusion, as can be seen in Table 9 and Figure 47 the currently best electromagnetic performance was achieved at a temperature of 800°C and an annealing duration of 15 minutes, achieving a resistivity of 33.773 $\Omega \cdot mm^2 \cdot m^{-1}$ and a coercivity of 169 A/m.

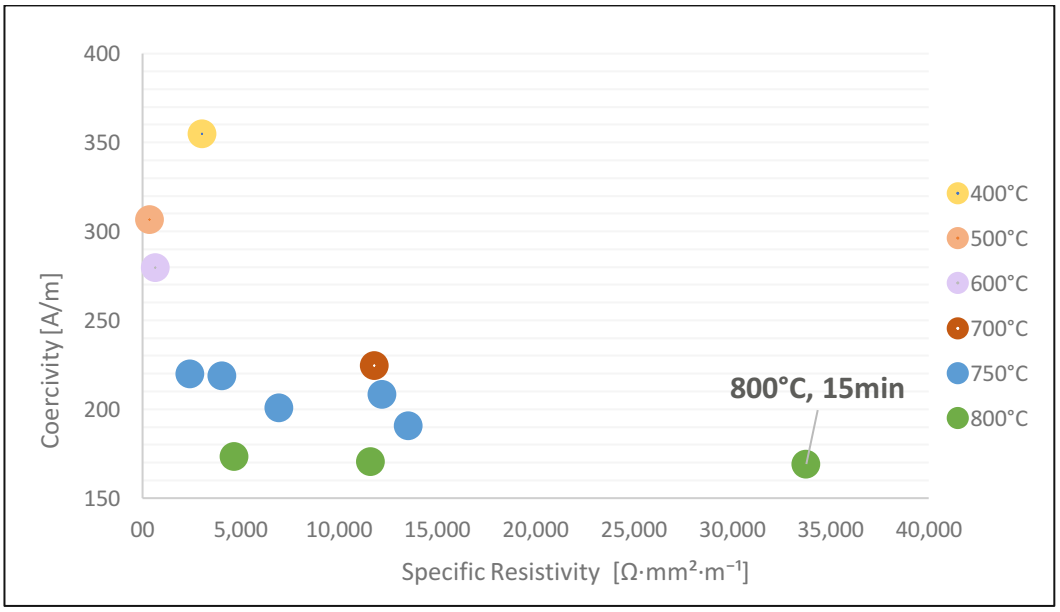

Figure 47 Performance of the samples at different annealing temperatures and durations

5.5 Transverse Rupture Strength

The TRS was measured only on impregnated samples (as described in chapter 3.5). prepared with 0.75% paraffin at 400 MPa.

The annealing treatment does not seem to have a significant impact on the TRS values (see Figure 48 and Figure 49). Only the samples annealed at 400°C show a significantly lower TRS (see Figure 48). At this temperature, the paraffin might not be fully evaporated from the samples, as it has a boiling point above 300°C and probably effects the thorough distribution of the adhesive [38].

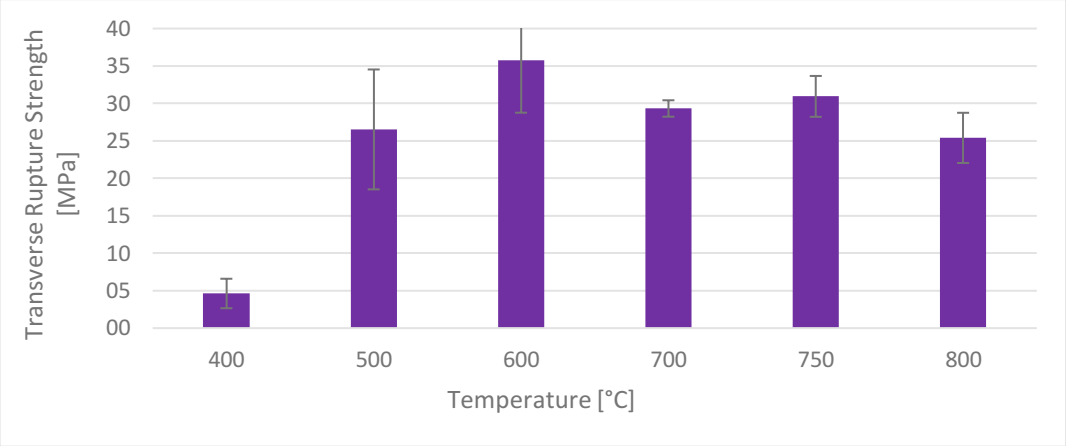

Figure 48 Transverse Rupture Strength of the samples at different temperatures

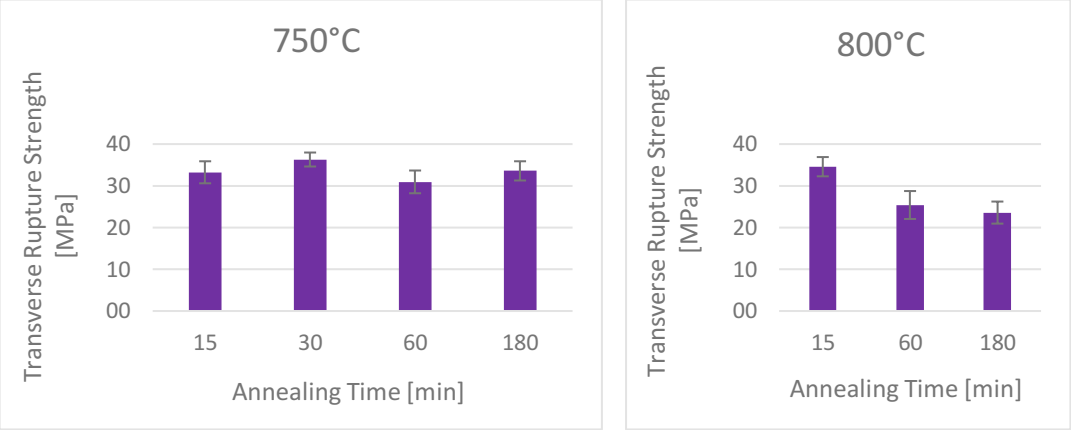

Figure 49 Transverse Rupture Strength at different annealing duration

6 Conclusion

The Fe-Si powder was characterised concerning composition and shape.

It was found that the powder particles exhibit a spherical shape and a relatively high hardness, which is poorly suited for powder compaction and therefore poses a challenge concerning compaction and stability of the samples.

Different methods of pressing the powder to compacted samples were tried. Two approaches were able to produce samples that exhibit at least enough stability for further measurements:

- Using paraffin as pressing aid
- Mixing with Somaloy 130i 5P

The effects of the amount of paraffin or the addition of Somaloy 130i 5P powder were compared regarding density, magnetic properties (coercivity and saturation magnetisation) and electric resistivity.

Sufficient stability of the samples can be achieved by adding a low-viscosity adhesive. Therefore, a method was developed to produce stable and practically applicable samples with a TRS of 31 ± 4.5, which is higher than usual Fe-powder pressed materials.

Still, the produced samples show a rather low density, which subsequently leads to a lower saturation magnetisation. This will have a negative impact on electromagnetic parts produced with the presented route, as the pieces will have to be produced at bigger sizes to compensate the low saturation magnetisation.

Furthermore, the effect of different annealing treatments, varied in annealing temperature and duration, was investigated (summarised in Table 10). With improvement of the heat treatment specific resistivity values above 30000 $\Omega \cdot mm^2 mm^{-1}$ were reached while simultaneously showing a coercivity of about 170 A/m. These results show that the produced samples are able to compete with other commercially available SMC powders (e.g. Somaloy 130i 5P [39]).

A theory was proposed for the high increase in electrical resistivities of the samples annealed at high temperatures. The building of an insulating coating of SiO_2 during the heat treatment was suggested, which was confirmed by XPS measurements.

Annealing Temperature [°C]	Annealing Duration [min]	Saturation magnetisaion [µT*m³/kg]	Coercivity [A/m]	Specific Resistivity (after impregnation) [Ω·mm²·m⁻¹]
400	60	210	355	3035
500	60	212	307	348
600	60	213	280	656
700	60	212	225	11809
	15	211	220	2423
	30	216	219	4051
750	60	216	201	6957
	180	214	209	12185
	300	210	191	13513
	15	214	169	33773
800	30	215	173	4669
	60	214	170	11609

Table 10 Properties of the final samples with the best performance

7 References

1. Krings, A., et al., *Characteristics Comparison and Selection Guide for Magnetic Materials used in Electrical Machines.* 2015 Ieee International Electric Machines & Drives Conference (Iemdc), 2015: p. 1152-1157.
2. Schoppa, A. and P. Delarbre, *Soft Magnetic Powder Composites and Potential Applications in Modern Electric Machines and Devices.* Ieee Transactions on Magnetics, 2014. **50**(4).
3. Šalak, A., *Ferrous Powder Metallurgy*. 1995: Cambridge International Science Pub.
4. Black, J.T. and R.A. Kohser, *DeGarmo's Materials and Processes in Manufacturing*. 2011: Wiley.
5. C. Suryanarayana, E.I., *Mechanochemical Synthesis of Nanocrystalline Metal Powders*, in *Advances in Powder Metallurgy*, I.Z. Chang, Y., Editor. 2013, Woodhead Publishing: Oxford/Cambridge/Philadelphia/New Delhi. p. 42-68.
6. Dunkley, J.J., *Advances in atomisation techniques for the formation of metal powders*, in *Advances in Powder Metallurgy*, I.Z. Chang, Y., Editor. 2013, Woodhead Publishing: Oxford/Cambridge/Philadelphia/New Delhi. p. 3 - 18.
7. Slotwinski, J.A., et al., *Application of Physical and Chemical Characterization Techniques to Metallic Powders.* 40th Annual Review of Progress in Quantitative Nondestructive Evaluation: Incorporating the 10th International Conference on Barkhausen Noise and Micromagnetic Testing, Vols 33a & 33b, 2014. **1581**: p. 1184-1190.
8. Riedel, E., *Anorganische Chemie*. 6. Aufl.. ed. 2004, Berlin, Boston: de Gruyter.
9. Bas, J.A., J.A. Calero, and M.J. Dougan, *Sintered soft magnetic materials. Properties and applications.* Journal of Magnetism and Magnetic Materials, 2003. **254**: p. 391-398.
10. Muljadi, P. Sardjono, and S.J.E. Procedia, *Preparation and Characterization of 5 wt.% Epoxy Resin Bonded Magnet NdFeB for Micro Generator Application.* 2015. **68**: p. 282-287.
11. Coey, J.M.D., *Magnetism and Magnetic Materials*. 2010, New York: Cambridge University Press.
12. Oikonomou, C., *On Surface Characteristics and Microstructural Development of Soft Magnetic Composite Powder and Components*. Dissertation, 2015, Chalmers University of Technology: Gothenburg, Sweden.
13. *https://www.grandviewresearch.com/industry-analysis/soft-magnetic-materials-market*. 08.09.2020].
14. Boehm, A. and I. Hahn, *Comparison of Soft Magnetic Composites (SMCs) and electrical steel.* 2012 2nd International Electric Drives Production Conference (Edpc), 2012.
15. Cullity, B.D. and C.D. Graham, *Introduction to magnetic materials*. 2nd . ed. 2015, Hoboken, New Jersey: IEEE/Wiley.
16. Hornbogen, E., H. Warlimont, and B. Skrotzki, *Metalle: Struktur und Eigenschaften der Metalle und Legierungen*. 2019, Berlin / Heidelberg: Springer
17. You, D. and H. Park, *Developmental Trajectories in Electrical Steel Technology Using Patent Information.* Sustainability, 2018. **10**(8).
18. Schoppa, A., *Fertigungstechnische Herausforderungen bei weichmagnetischen Pulverwerkstoffen*, in *29. Hagener Symposium Pulvermetallurgie*, H. Kolaska, Editor. 2013, Pulvermetallurgie in Wissenschaft und Praxis. p. 231-247.
19. Simchi, A. and H. Danninger, *Electrical conductivity and microstructure of sintered ferrous materials: sintered iron.* Powder metallurgy, 2000. **43**(3): p. 209--218.
20. Zhao, G.L., C. Wu, and M. Yan, *Evolution of the insulation matrix and influences on the magnetic performance of Fe soft magnetic composites during annealing.* Journal of Alloys and Compounds, 2016. **685**: p. 231-236.

21. Shokrollahi, H. and K. Janghorban, *Different annealing treatments for improvement of magnetic and electrical properties of soft magnetic composites.* Journal of Magnetism and Magnetic Materials, 2007. **317**(1-2): p. 61-67.
22. Taghvaei, A.H., et al., *Influence of particle size and compaction pressure on the magnetic properties of iron-phenolic soft magnetic composites.* Journal of Physics and Chemistry of Solids, 2010. **71**(1): p. 7-11.
23. Hemmati, I., H.R.M. Hosseini, and A. Kianvash, *The correlations between processing parameters and magnetic properties of an iron-resin soft magnetic composite.* Journal of Magnetism and Magnetic Materials, 2006. **305**(1): p. 147-151.
24. Grande, M.A., et al., *New SMC Materials for Small Electrical Machine With Very Good Mechanical Properties.* Ieee Transactions on Industry Applications, 2018. **54**(1): p. 195-203.
25. Shokrollahi, H. and K. Janghorban, *Soft magnetic composite materials (SMCs).* Journal of Materials Processing Technology, 2007. **189**(1-3): p. 1-12.
26. Mascarenhas, J.M.G., *Powder Metallurgy: A Major Partner of the Sustainable Development.* Materials Science Forum, 2004. **455-456**: p. 857-860.
27. Gierl-Mayer, C., *Personal communication*. 2020.
28. Ouda, K., *Unpublished Work*. 2019.
29. *https://www.sigmaaldrich.com/technical-documents/articles/biology/ir-spectrum-table.html*. 24.09.2020].
30. Launer, P., *Infrared Analysis of Organosilicon Compounds*, in *Silicon Compounds: Silanes & Silicones*, B. Arkles and G.L. Larson, Editors. 2013, Gelest Inc.: Morrisville, PA. p. 175-178.
31. *http://www.xpsfitting.com/*. 08.09.2020].
32. *https://xpssimplified.com/*. 08.09.2020].
33. Wu, S., et al., *Magnetic properties of iron-based soft magnetic composites with SiO2 coating obtained by reverse microemulsion method.* Journal of Magnetism and Magnetic Materials, 2015. **381**: p. 451-456.
34. Sze, S.M. and K.K. Ng, *Physics of semiconductor devices, third edition*. 3rd ed. 2006, Hoboken, NJ: Wiley.
35. Haynes, W.M., *CRC Handbook of Chemistry and Physics, 93rd Edition*. 2012, Baton Rouge: CRC Press LLC.
36. Biesinger, M.C., et al., *Resolving surface chemical states in XPS analysis of first row transition metals, oxides and hydroxides: Sc, Ti, V, Cu and Zn.* Applied Surface Science, 2010. **257**(3): p. 887--898.
37. Schatt, W., B. Kieback, and K.-P. Wieters, *Pulvermetallurgie: Technologien und Werkstoffe*. 1. Aufl. ed. VDI-Buch. 2007, Berlin/Heidelberg/New York: Springer-Verlag.
38. Mózes, G., et al., *Paraffin Products: Properties, Technologies, Applications*. Developments in Petroleum Science. Vol. 14. 1983, Budapest: Elsevier Science.
39. https://www.hoganas.com/globalassets/download-media/sharepoint/brochures-and-datasheets---all-documents/somaloy-5p_material-data_june_2018_2274hog.pdf. 24.09.2020]